Frontiers in Bioscience
Landmark

Front. Biosci. (Landmark Ed) **2026**; 31(3): 48929
https://doi.org/10.31083/FBL48929

Original Research

Comprehensive Analysis of N7-Methylguanosine-Modified Long Non-Coding RNAs Identifies *DPY19L1P1* as a Key Oncogenic Effector in Oral Squamous Cell Carcinoma

Kexin Liang[1,2,†], Hui Gong[1,2,†], Simiao Bian[1,2], Huiyang Xu[1,2], Rui Zang[1], Jiayi Hao[1], Yajie Wang[1], Yue Zhang[1], Yingying Jiang[1,2,*]

[1] School of Stomatology, Shandong Second Medical University, 261053 Weifang, Shandong, China
[2] Weifang Key Laboratory of Oral Biomedicine, Shandong Second Medical University, 261053 Weifang, Shandong, China
*Correspondence: jiangyy@sdsmu.edu.cn (Yingying Jiang)
[†] These authors contributed equally.

Academic Editor: Amancio Carnero Moya
Submitted: 9 December 2025 Revised: 10 February 2026 Accepted: 25 February 2026 Published: 9 March 2026

Abstract

Background: N7-methylguanosine (m7G) is an important RNA modification involved in the regulation of gene expression during transcription. While its roles in mRNAs and tRNAs are increasingly understood, the distribution and function of m7G in long non-coding RNAs (lncRNAs), particularly in oral squamous cell carcinoma (OSCC), remain poorly understood. This study aimed to systematically characterize the m7G methylation landscape of lncRNAs in OSCC and investigate the oncogenic function and regulatory mechanism of the m7G-modified lncRNA *DPY19L1P1*. **Methods**: Methylated RNA immunoprecipitation sequencing (MeRIP-seq) and RNA sequencing (RNA-seq) were performed on three pairs of OSCC and adjacent normal tissues to identify differentially m7G-modified and differentially expressed lncRNAs. Motif prediction, its potential functions are identified through analysis of Gene Ontology (GO) and Kyoto Encyclopedia of Genes and Genomes (KEGG) pathways. *DPY19L1P1* was prioritized based on its high level of m7G modification and upregulation. Its clinical relevance was assessed using TCGA-HNSC datasets. *In vitro* and *in vivo* functional assays were performed to evaluate its oncogenic roles. The regulatory effects of methyltransferase-like 1 (METTL1) and WD repeat domain 4 (WDR4) on *DPY19L1P1* were examined using expression correlation, MeRIP quantitative real-time PCR (qPCR), and splicing efficiency analyses. **Results**: A total of 5486 OSCC-specific m7G peaks and 5135 modified lncRNAs were identified. Compared to normal tissues, OSCC tissues exhibited broader distribution and higher levels of m7G modifications. Among 15,085 hyper-m7G-modified lncRNAs detected in OSCC, 80 were also upregulated. They are enriched in metabolic pathways associated with lncRNA cell adhesion and migration. *DPY19L1P1* displayed the most prominent m7G methylation and expression levels, and was significantly associated with advanced clinical stage and poor differentiation, indicating its diagnostic potential. Mechanistically, METTL1 and WDR4 cooperatively enhanced both the m7G modification and expression of *DPY19L1P1* by promoting its splicing efficiency. Furthermore, METTL1/WDR4 and *DPY19L1P1* synergistically promoted OSCC progression, with *DPY19L1P1* functioning as a key downstream effector. Functionally, *DPY19L1P1* facilitated OSCC cell proliferation, migration, glycolysis-driven metabolic reprogramming, and epithelial–mesenchymal transition (EMT). **Conclusion**: This study provides a comprehensive profile of m7G-modified lncRNAs in OSCC and identifies *DPY19L1P1* as a hyper-m7G-modified oncogenic lncRNA regulated by the METTL1/WDR4 complex. As a key downstream effector, *DPY19L1P1* promotes OSCC progression through metabolic reprogramming and EMT, and may serve as a potential diagnostic biomarker and therapeutic target.

Keywords: oral squamous cell carcinoma; N7-methylguanosine; long non-coding RNAs; DPY19L1P1; METTL1; WDR4

1. Introduction

Oral squamous cell carcinoma (OSCC) constitutes the majority of head and neck squamous cell carcinoma (HNSCC), and ranks as a frequently diagnosed neoplasm in the oral cavity [1]. Owing to its propensity for recurrence, therapeutic resistance, and strong invasiveness, patients with OSCC often experience poor prognosis and high disability rates, severely affecting their quality of life [2]. In the present, the initial implementation of the OSCC policy is being implemented, radiotherapy, targeted therapy, immunotherapy [2,3]. However, because of significant tumor heterogeneity, clinical outcomes have not improved substantially in recent years. Thus, it is clinically imperative to decipher the biological basis driving OSCC progression and to pinpoint potential targets for treatment.

In recent years, RNA epigenetic modifications have emerged as critical regulators of gene expression and have attracted increasing attention in cancer research. Among them, N1-methyladenosine (m1A), 5-methylcytosine (m5C), N6-methyladenosine (m6A), N7-methylguanosine (m7G) represent the major types of RNA modification [4]. Among these, m7G is a conserved and functionally diverse post-transcriptional modification, in which a methyl group is added to the N7 position of guanine in RNA, catalyzed by specific methyltransferases [5]. Classically, m7G is recognized as a hallmark modification at the 5′ cap of mRNAs and within tRNAs [6,7], but also within internal regions of mRNA and long non-coding RNAs (lncRNAs) [8,9], as well as in ribosomal RNAs [10], microRNAs [11]. m7G regulates various aspects of RNA metabolism, including methylation, splicing, nuclear export, stability, and translation, thereby playing crucial roles in maintaining cellular homeostasis and promoting cancer progression [12]. The m7G modification reaction primarily depends on the activity of known methyltransferase complexes [7,11]. Specifically, METTL1 and WDR4 heterodimer acts as a critical writer complex that mediates the deposition of m7G at internal RNA sites [13]. Previous studies have shown that METTL1 and WDR4 are overexpressed in multiple cancer types and are positively correlated in their expression levels. In HNSCC, their synergistic upregulation drives tumor advancement and implies an adverse clinical prognosis [7,14].

LncRNAs are a large category of noncoding RNAs with lengths greater than 200 nucleotides but no protein-coding ability [15]. Emerging studies have revealed that lncRNAs can modulate OSCC progression by controlling biological processes including cell proliferation, apoptosis, and metabolic reprogramming [16,17]. Notably, certain highly expressed m7G-modified lncRNAs have been closely correlated with poor prognosis in OSCC [18], suggesting their potential as functional molecules or biomarkers. However, the specific roles and mechanisms of m7G-modified lncRNAs in OSCC remain largely unexplored and warrant further investigation through integrative omics and functional studies.

In this work, we systematically characterized the m7G methylation landscape of lncRNAs in OSCC by integrating m7G methylated RNA immunoprecipitation sequencing (MeRIP-seq) with RNA-seq. Gene Ontology (GO) and Kyoto Encyclopedia of Genes and Genomes (KEGG) enrichment analyses were conducted to explore the biological pathways potentially regulated by m7G-modified lncRNAs. We identified a subset of lncRNAs that were both hyper-m7G-modified and upregulated in OSCC. Among them, *DPY19L1P1* was prioritized as a representative candidate due to its most prominent m7G hypermethylation, marked upregulation and strong association with clinicopathological features. METTL1/WDR4 was found to positively regulate both the expression and m7G modification of *DPY19L1P1*. Functionally, *DPY19L1P1* facilitates OSCC cell proliferation, migration, glycolysis-driven metabolic reprogramming and EMT, acting as a key downstream effector of METTL1/WDR4-mediated epitranscriptomic regulation. These findings highlight *DPY19L1P1* as a promising diagnostic biomarker and promising drug target, and provide novel insight into the oncogenic roles of m7G-modified lncRNAs in OSCC.

2. Materials and Methods

2.1 Tissue Collection and Cell Resources

Six tissue samples (C1/N1, C2/N2, and C3/N3) were collected from three OSCC patients at the First Affiliated Hospital of Shandong Second Medical University (formerly Weifang Medical University). The criteria and procedures for tissue collection were detailed in our previous studies, and the study was approved by the Ethics Committee of Shandong Second Medical University (formerly Weifang Medical University) [19,20]. Human OSCC cell lines (HN30, CAL-27, HN6, SCC-25 and SCC-9) were obtained from Shanghai Ninth People's Hospital, Shanghai Jiao Tong University School of Medicine. The cDNA samples of normal primary human oral mucosal epithelial cells were provided by the same institution. All procedures related to these samples were conducted under institutional ethical approval (Approval No. SH9H-2019-TK235-1) with informed consent obtained from donors. The characterization of these cells has been previously reported [21,22]. All cell culture conditions and protocols were consistent with those used in our earlier publication [20]. All procedures in this study were performed in accordance with the Declaration of Helsinki. All cell lines were recently verified prior to use by short tandem repeat (STR) analysis performed by Shanghai Biowing Applied Biotechnology Co., Ltd. All cell lines tested negative for mycoplasma.

2.2 Methylated RNA Immunoprecipitation Sequencing (MeRIP-seq)

The sequencing process was described in a previous study [19]. In brief, the MeRIP-seq technique involves the use of an m7G-specific antibody to enrich m7G-modified lncRNA fragments, followed by high-throughput sequencing to locate and quantify m7G modifications on the RNA fragments.

2.3 Differential Analysis of lncRNA Molecules Based on Methylation Levels and Expression Levels

A quality score threshold of Q30 was applied for quality control following sequencing on the Illumina NovaSeq 6000 platform. Cutadapt software (v2.10; Marcel Martin, Max Planck Institute for Molecular Genetics, Berlin, Germany) was utilized to generate high-quality, clean reads [23]. Clean reads from all samples were mapped to the reference genome using HISAT2 (v2.0.4, Johns Hopkins University, Baltimore, MD, USA) [24]. Methylated sites were called using MACS3 (v3.0.3, Harvard University, Cambridge, MA, USA) with the default parameters, and the p values of the peaks were calculated based on the Poisson distribution [25]. Differentially methylated sites were called using DiffReps software (v1.55.6, The University of Texas MD Anderson Cancer Center, Houston, TX, USA), with p values computed via negative binomial regression [26]. Peaks located in the exons of the lncRNAs were extracted for annotations, and differentially methylated lncRNAs were identified using the thresholds of fold change (FC) >2 and adjusted $p < 0.05$.

For transcriptomic analysis, high-quality reads were mapped to the human reference genome (UCSC HG19) using HISAT2 (v2.0.4) [24]. Transcript-level raw counts were generated using HTSeq (v0.9.1, European Molecular Biology Laboratory, Heidelberg, Germany), and lncRNA expression profiles were analyzed [27]. Differential expression analysis between OSCC and normal tissues was performed using edgeR (v3.16.5, Walter and Eliza Hall Institute of Medical Research, Melbourne, VIC, Australia) [28], with thresholds set at FC >2 and adjusted $p < 0.05$.

p-values for both MeRIP-seq and RNA-seq analyses were adjusted for multiple testing using the Benjamini-Hochberg method, and an adjusted p-value < 0.05 was considered statistically significant.

2.4 Bioinformatics Analysis

GO and KEGG pathway enrichment analyses on genes associated with differentially m7G-modified and differentially expressed lncRNAs were analyzed using the online tool, Database for Annotation, Visualization, and Integrated Discovery (DAVID, https://davidbioinformatics.nih.gov/) [29]. The analyses were conducted based on the *Homo sapiens* genome reference (HG19). A statistically meaningful difference was defined as $p < 0.05$. The top GO and KEGG terms were ranked by enrichment score [$-\log_{10}(p)$] and presented accordingly.

To visualize the chromosomal distributions of m7G-modified lncRNAs in OSCC versus normal tissues, the RCircos package (v1.2.2, National Cancer Institute, Bethesda, MD, USA) in R was utilized [30]. In addition, sequence motif characterization of m7G modifications in lncRNAs was performed with DREME (v5.5.9, University of Washington, Seattle, WA, USA) software [31].

2.5 Total RNA Extraction and Quantitative Real-Time PCR (qPCR)

Total RNA was isolated from cultured cells using TRIzol reagent (M5101, NCM Biotech, Co., Ltd., Suzhou, Jiangsu, China). cDNA was generated by reverse transcription with the Evo M-MLV RT Kit (AG11705, Accurate Biology Co., Ltd., Changsha, Hunan, China). The target RNAs were amplified with the SYBR Green Pro Taq HS qPCR Kit (AG11701, Accurate Biology Co., Ltd., Changsha, Hunan, China). Gene expression levels were normalized to the β-actin internal control using the $2^{-\Delta\Delta ct}$ method. The sequences of all primers used are provided in **Supplementary Table 1**.

2.6 Nuclear/Cytoplasmic Fractionation

RNA from nuclear and cytoplasmic fractions was extracted using the PARIS™ Kit (AM1921, Thermo Fisher Scientific, Waltham, MA, USA) following the manufacturer's instructions. β-actin was used as the internal control for cytoplasmic RNA, while U6 served as the reference for nuclear RNA. Detailed primer sequences are provided in **Supplementary Table 1**.

2.7 Fluorescence In Situ Hybridization (FISH)

Fluorescence-labeled probes targeting *DPY19L1P1*, *U6*, and *18S* rRNA were commercially designed and produced by RiboBio (Guangzhou, China). FISH was performed using the Ribo™ Fluorescent *In Situ* Hybridization Kit (C10910, RiboBio Co., Ltd., Guangzhou, Guangdong, China). Briefly, HN30 cells were cultured on sterile glass coverslips, fixed with 4% paraformaldehyde for 10 min, and permeabilized with 0.5% Triton X-100. After prehybridization, cells were incubated with fluorescent probes at 37 °C overnight. The next day, excess probes were removed by washing, and nuclei were counterstained with DAPI. Coverslips were mounted using an antifade reagent, and fluorescence images were captured using a TCS SP8 laser scanning confocal microscope (version 3.7.5, Leica Microsystems, Germany). Image processed with LAS X software (Leica Microsystems, Wetzlar, Germany) to determine the subcellular localization of *DPY19L1P1*.

2.8 MeRIP-qPCR

MeRIP was conducted using the GenSeq® m7G MeRIP Kit (GS- ET-004A, CloudSeq Inc., Shanghai, China) to assess the m7G modification levels of the specific transcripts. Initially, total RNA was treated with mRNA Decapping Enzyme (M0608S, New England Biolabs, Ipswich, MA, USA) to remove the 5′ cap structure. The RNA was then fragmented, and 3 µg of the fragmented RNA was reserved as the input control. The remaining RNA was mixed with either anti-m7G antibody or control IgG, both pre-bound to Protein A/G magnetic beads were added, and the mixture was incubated at 4 °C for 1 hour. After immunoprecipitation, the beads were washed with 1× IP buffer, and the bound RNA was purified using RLT buffer. Both input and m7G-enriched RNA fractions were reverse transcribed, followed by qPCR to quantify m7G enrichment.

2.9 Small Interfering RNA (siRNA), Smart Silencer (SS) and Plasmid Transfection

siRNAs targeting METTL1 and WDR4 (si-METTL1 and si-WDR4), as well as Smart Silencer RNAs targeting *DPY19L1P1* (SS-DPY19L1P1), were synthesized by RiboBio (Guangzhou, China). The target sequences are provided in **Supplementary Table 2**. Expression plasmids for METTL1, WDR4 and *DPY19L1P1* were constructed by GeneChem Co., Ltd. (Shanghai, China). Cells were transfected using the Lipo8000TM reagent (Beyotime, Shanghai, China) following the protocol. qPCR was used to evaluate transfection efficiency.

2.10 Cell Counting Kit-8 (CCK-8) Assay

Cells (1.5 × 10^3 cells/well) transfected with the SS-DPY19L1P1 or DPY19L1P1 plasmid for 24 h were plated in triplicate into 96-well plates. Following incubation, 10 µL of CCK-8 solution (CK04, Dojindo Laboratories, Kumamoto, Japan) was added to each well, and the plates were incubated at 37 °C with 5% CO_2 for 2 hours. Cell viability was assessed daily for five consecutive days by measuring the optical density at 450 nm with a microplate reader (Thermo Fisher Scientific, Waltham, MA, USA).

2.11 Transwell Migration Assay

The cells (2.5 × 10^4 cells/well) transfected with the SS RNA/expression plasmid for 24 h were seeded into the upper chamber in 150 µL of serum-free DMEM (YR-PHE, Shanghai, China). Subsequently, the lower chamber was filled with DMEM containing 10% fetal bovine serum to support cell growth, and the cells were incubated at 37 °C and 5% CO_2 for 24–48 h. After fixation with 4% paraformaldehyde solution (Beyotime), the cells were stained with 0.5% Crystal Violet Staining Solution (C0121, Beyotime Biotech Inc., Shanghai, China). Five fields of view were randomly selected for imaging using a Leica S8 APO Stereomicroscope (Leica Microsystems CMS GmbH, Wetzlar, Germany).

2.12 Subcutaneous Xenograft Tumor Model in Nude Mice

Twelve 4-week-old BALB/c nude mice (Jinan Pengyue Experimental Animal Breeding Center, SCXK [Lu] 2019-0003) were randomly assigned into two groups (n = 6 per group). All animal studies received approval from the Animal Care and Use Committee of Weifang Medical University (Approval No. 2023SDL332). Due to institutional restructuring, the committee has been renamed the Animal Care and Use Committee of Shandong Second Medical University, and the original approval remains valid under the same protocol.

To establish the subcutaneous xenograft tumor model, CAL-27 cells (2 × 10^7 cells/mL) were injected subcutaneously (100 µL) into the dorsal area near the forelimbs on both sides of each mouse. One week after inoculation, mice received intratumoral injections of 5 nmol/50 µL cholesterol- and methylation-modified DPY19L1P1-targeting antisense oligonucleotide (ASO-DPY19L1P1) or ASO-NC every 4 days, for a total of five injections. The ASO-DPY19L1P1 sequence was derived from the most effective candidate identified in the SS-DPY19L1P1 screening and was synthesized by RiboBio (Guangzhou, China) with cholesterol and methylation modifications to enhance *in vivo* stability and transfection efficiency. This method of *in vivo* transfection in animal models has been documented in the previous studies [32].

Following 28 days, euthanasia was performed on mice under anesthesia via an intraperitoneal injection of sodium pentobarbital (150 mg/kg; prepared as a 50 mg/mL solution, Sigma-Aldrich, St. Louis, MO, USA), with death confirmed by the absence of heartbeat and respiration. Cervical dislocation was applied as a secondary measure if necessary. All procedures adhered to the AVMA Guidelines for the Euthanasia of Animals (2020).

Following euthanasia, tumors were excised, photographed, and measured to compare tumor volume and weight between the two groups. The tumor tissues underwent fixation in 4% paraformaldehyde for 24 hours, followed by dehydration, paraffin embedding, and sectioning. Histological analysis was conducted using Hematoxylin and Eosin (H&E) staining, while immunohistochemistry with a Ki-67 antibody was employed to assess cellular proliferation. The stained tissue sections were visualized and captured using an upright light microscope.

2.13 RNA Splicing Efficiency Assay

To evaluate the splicing efficiency of *DPY19L1P1*, qPCR was performed using two sets of transcript-specific primers, one amplifying unspliced precursor RNA (targeting intronic regions or exon-intron junctions) and the other amplifying spliced mature RNA (targeting exon-exon junctions). Splicing efficiency was quantified as the ratio of mature RNA to precursor RNA, and changes in this ratio were used to indicate alterations in splicing efficiency.

2.14 ATP Assay

ATP levels in CAL-27 and HN30 cells were measured using an ATP Content Assay Kit (Cat# BC0300, Solarbio, Beijing, China) according to the manufacturer's instructions. In brief, the cells were harvested and resuspended in the lysis buffer (1 mL per 10^7 cells). After homogenization and full lysis on ice, the samples were centrifuged at 10,000 ×g for 10 minutes at 4 °C, after which the supernatants were collected. For quantification, 100 µL of 0.625 µmol/mL ATP standard solution or cell lysate was added to a 1 mL quartz cuvette containing 640 µL of working reagent and 260 µL of reagent I. The reaction mixture underwent incubation at 37 °C for 10 min. Absorbance was then measured at 340 nm using a UV spectrophotometer. ATP concentrations were derived from a standard curve and are expressed as µmol per 10^6 cells.

2.15 Glucose Uptake Assay

Glucose uptake was quantified with a commercial Glucose Assay Kit (A154-1-1, Nanjing Jiancheng Bioengineering Institute, Nanjing, China) following the manufacturer's protocol. Cells were seeded in 6-well plates and subjected to the indicated treatments. After 24–48 h, culture supernatants were collected and centrifuged at 12,000 ×g for 10 min. Glucose concentrations were measured using the glucose oxidase-peroxidase (GOD-POD) method, and absorbance was detected at 505 nm. Glucose consumption was determined as the difference between the concentration in blank medium and the residual concentration in the experimental groups, and was normalized to cell number or total protein content.

2.16 Lactate Production Assay

Lactate levels in culture media were quantified using the L-Lactic Acid (LA) Colorimetric Assay Kit (E-BC-K044-M, Elabscience Biotechnology Inc., Wuhan, Hubei, China) following the manufacturer's protocol. After treatment or transfection, culture supernatants were collected and centrifuged at 12,000 ×g for 10 minutes to remove debris. Dilute an appropriate amount of the supernatant, then add lactate assay buffer and color development reagent. Incubate at 37 °C for 10 minutes. Measure absorbance at 530 nm using a microplate reader. Calculate lactate concentration based on the standard curve and normalize to cell number or total protein concentration.

2.17 Western Blotting

Western blotting was carried out as previously described [22]. Antibodies employed in this study are listed in **Supplementary Table 3**. HRP-conjugated goat anti-mouse IgG (H+L) (Cat# P8001) and goat anti-rabbit IgG (H+L) (Cat# P8002) were purchased from New Cell and Molecular (NCM) Biotech (Suzhou, Jiangsu, China) and used as secondary antibodies at a 1:10,000 dilution. Immunoreactivity was visualized with enhanced chemiluminescence (ECL) Ultra reagent (NCM Biotech, Suzhou, Jiangsu, China). Band intensities were measured using ImageJ software, and the relative protein expression levels were analyzed accordingly.

2.18 Statistical Analysis

All statistical analyses were performed using SPSS version 16.0 (IBM Corp., Armonk, NY, USA) and GraphPad Prism version 10.0 (GraphPad Software, San Diego, CA, USA). For comparisons between two groups, an unpaired Student's *t*-test was used. Differences among more than two groups were assessed using one-way analysis of variance (ANOVA) followed by post hoc tests as appropriate. Pearson's correlation analysis was conducted to evaluate the relationships between gene expression levels. All data are expressed as mean ± standard deviation (SD), and p-values < 0.05 were considered statistically significant unless otherwise noted.

3. Results

3.1 Comprehensive Landscape of m7G-Modified lncRNAs in OSCC and Normal Tissues

To explore the m7G methylation landscape in OSCC, m7G MeRIP-seq analysis was performed on three OSCC tissue samples (C1, C2, C3) and three matched adjacent normal tissue (N1, N2, N3). For high-confidence identification, only m7G peaks and lncRNAs detected in at least two biological replicates per group were included in subsequent analyses.

In OSCC tissues, a total of 1672 m7G peaks and 5651 modified lncRNAs were commonly detected across three samples (Fig. 1A,B). In comparison, 1220 shared m7G peaks and 5903 m7G-modified lncRNAs were identified in normal tissues (Fig. 1C,D).

Upon integrating the OSCC and normal datasets, we found that 5486 m7G peaks and 5135 lncRNAs were specific to OSCC, while 2312 m7G peaks and 8646 m7G-modified lncRNAs were shared between the two groups (Fig. 1E,F). This finding highlights that m7G methylation in OSCC encompasses both conserved and tumor-specific modification patterns, suggesting its potential involvement in OSCC-specific transcriptional regulation.

A Circos plot, generated using the Circos package in R, revealed the chromosomal localization of m7G peaks in both OSCC and normal tissues (Fig. 1G). These peaks were located predominantly on chromosomes 1, 17, and 19 (Fig. 1H). To further characterize the m7G modification landscape, we analyzed the distribution of m7G peaks per lncRNA. In normal tissues, the majority of m7G-modified lncRNAs (approximately 75%) harbored only a single peak. In contrast, although 50.13% of lncRNAs in OSCC tissues also carried a single m7G peak, a substantially higher proportion exhibited multiple peaks—nearly 50% had two or more. This shift suggests an increase in methylation complexity in lncRNAs during OSCC tumorigenesis (Fig. 1I). Additionally, the peak length distribution differed significantly between OSCC and normal tissues ($p < 0.0001$), with OSCC tissues exhibiting longer peak regions (Fig. 1J).

Motif analysis was conducted using DREME software to identify conserved sequence motifs within the m7G peaks. A total of six significantly enriched motifs were detected in each group (Fig. 1K). Among these, a conserved RGAAR motif (R = G/A) was predominantly enriched in OSCC tissues ($p = 2.4 \times 10^{-23}$, $E = 1.9 \times 10^{-18}$), whereas the CUGKR motif (K = G/U, R = G/A) was more frequently observed in normal tissues ($p = 4.9 \times 10^{-40}$, $E = 4.2 \times 10^{-35}$). Although some motifs were shared between cancer and normal groups, several were uniquely enriched in each, suggesting both common and distinct m7G recognition patterns. These findings are consistent with previously reported m7G motifs, further supporting their biological relevance in epitranscriptomic regulation.

3.2 Comprehensive Profiling of Differentially m7G-Methylated lncRNAs in OSCC

Based on their genomic locations, m7G-modified lncRNAs can be classified into six categories: exon sense-overlapping, intronic antisense, intergenic, natural antisense, intron sense-overlapping, and bidirectional. Among these, the majority of m7G-modified lncRNAs in both OSCC and normal tissues originated from exon sense-overlapping and intergenic regions (Fig. 2A). Comparative analysis of the distribution patterns revealed that m7G-modified lncRNAs in OSCC tissues (C1–C3) were signifi-

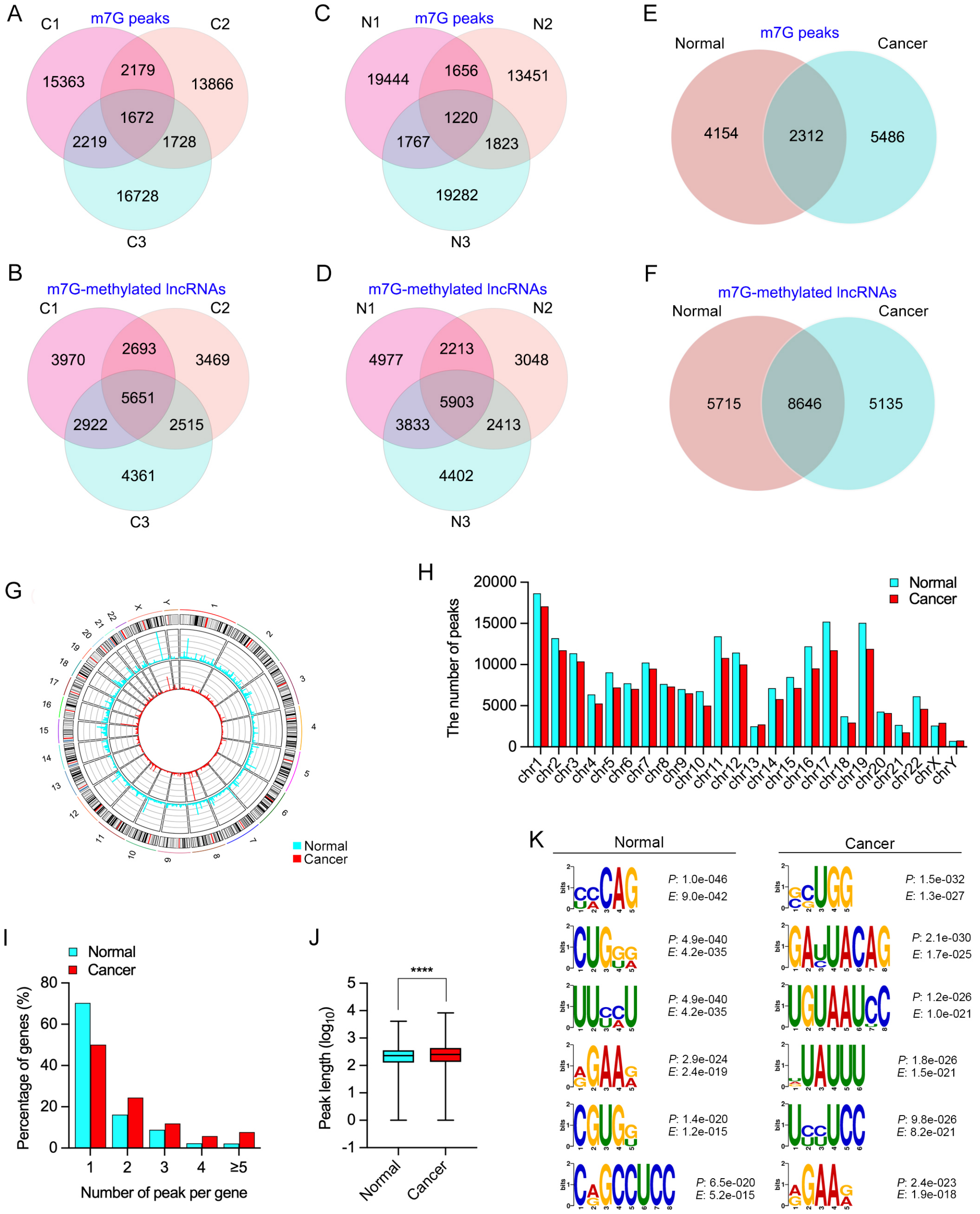

Fig. 1. Comprehensive landscape of m7G-modified lncRNAs in OSCC and normal tissues. (A,B) Venn diagrams showing the number of total m7G peaks (A) and m7G-modified lncRNAs (B) identified in OSCC tissues, based on the intersection of three OSCC samples (C1–C3), as analyzed by methylated RNA immunoprecipitation sequencing (MeRIP-seq). (C,D) Venn diagrams showing the number of total m7G peaks (C) and m7G-modified lncRNAs (D) identified in normal tissues (N1–N3), based on the overlap of three normal samples (N1–N3), also determined by MeRIP-seq. (E,F) Venn diagrams showing the overlap and specificity of m7G peaks (E) and m7G-modified lncRNAs (F) between OSCC and normal tissues. (G) Circos plot showing the chromosomal distribution of m7G-modified lncRNAs in OSCC and normal tissues. (H) Bar graph showing the number of m7G peaks across each chromosome in OSCC and normal tissues. (I) Distribution of the number of m7G peaks per lncRNA transcript in cancer and normal tissues. (J) Box plot comparing the length of m7G peaks ($\log_{10}$-transformed) between OSCC and normal tissues. (K) Top six significantly enriched sequence motifs within m7G peaks identified in normal and OSCC tissues, along with associated *p*-values and *E*-values. m7G, N7-methylguanosine; lncRNA, long non-coding RNA; OSCC, oral squamous cell carcinoma. ****$p < 0.0001$.

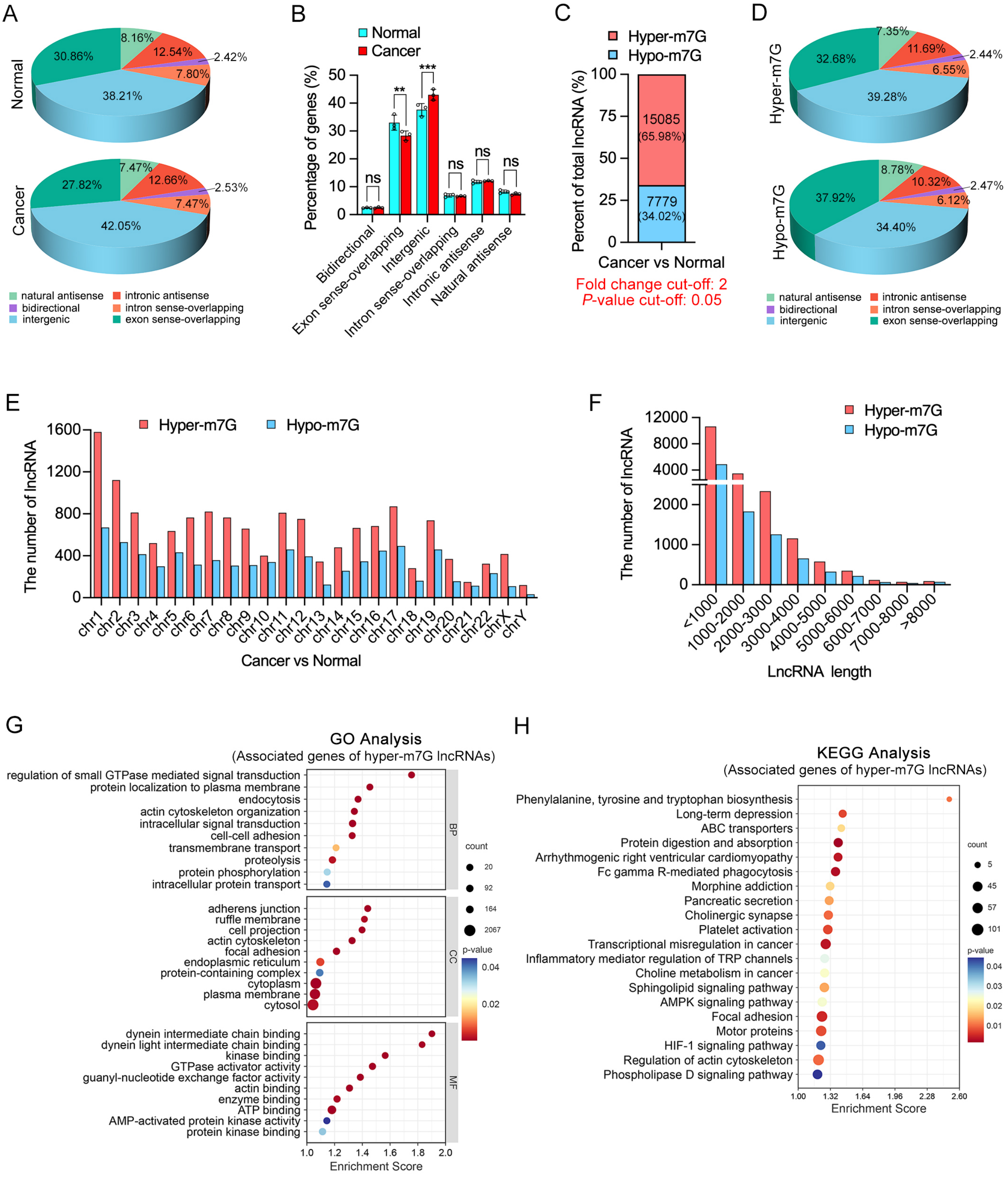

Fig. 2. Integrated characterization of differentially m7G-methylated lncRNAs in OSCC. (A,B) Genomic feature distribution of m7G-modified lncRNAs in normal (top) and OSCC (bottom) tissues. Pie charts (A) and bar graphs (B) showing the proportion of lncRNAs derived from 6 genomic regions. (C) Proportional analysis showing that 65.98% of differentially modified lncRNAs were hyper-m7G, while 34.02% were hypomethylated (hypo-m7G) in OSCC compared to normal tissues. (D) Genomic origin categorization of hyper- and hypo-m7G lncRNAs in OSCC tissues, revealing distinct distributions between the two methylation states. (E) Chromosomal distribution of hyper- and hypo-m7G lncRNAs across all chromosomes, with a broad but uneven genomic distribution. (F) Length distribution of lncRNAs with aberrant m7G modification. (G,H) GO and KEGG enrichment analyses of genes associated with hyper-m7G-modified lncRNAs in OSCC tissues. GO, Gene Ontology; BP, biological process; CC, cellular component; MF, molecular function; KEGG, Kyoto Encyclopedia of Genes and Genomes. $^{**}p < 0.01$, $^{***}p < 0.001$, ns, not significant.

cantly less enriched in exon sense-overlapping regions and more frequently derived from intergenic regions compared to those in normal tissues (N1–N3) (Fig. 2B).

To further investigate group-specific methylation differences, differentially m7G-methylated lncRNAs were identified using DiffReps software, with thresholds set at FC >2 and $p < 0.05$. A total of 15,085 hyper-m7G lncRNAs (65.98%) and 7779 hypo-m7G lncRNAs (34.02%) were identified in OSCC tissues compared to normal controls, indicating that m7G hypermethylation is the predominant epitranscriptomic alteration in OSCC (Fig. 2C). Further analysis of the genomic distribution showed that hyper-m7G lncRNAs were less frequently located in exon sense-overlapping regions and more enriched in intergenic regions compared to hypo-m7G lncRNAs (Fig. 2D), consistent with the overall group-wise differences shown in (Fig. 2B).

Additionally, analysis of the chromosomal localization of differentially m7G-modified lncRNAs revealed that hyper-m7G-modified lncRNAs were consistently more abundant than hypo-m7G-modified lncRNAs across all chromosomes (Fig. 2E). This distribution pattern was broadly consistent with the previously observed distribution of total m7G peaks, indicating potential chromosomal preferences of m7G modifications and possible links to transcriptional activity or regional genomic function. Moreover, analysis of transcript lengths revealed that lncRNAs shorter than 2000 nucleotides exhibited a higher frequency of both hyper- and hypo-m7G methylation events (Fig. 2F), suggesting that shorter lncRNAs may be more dynamically regulated by m7G methylation in OSCC (Fig. 2F).

To elucidate the potential biological functions of differentially m7G-methylated lncRNAs in OSCC, GO and KEGG enrichment analyses were performed based on their predicted target genes. The analysis focused on genes associated with hyper-m7G lncRNAs. All enrichment terms presented met the significance threshold of $p < 0.05$ and were ranked according to both gene count and enrichment score. GO analysis was performed across three categories: Biological Process (BP), Cellular Component (CC), and Molecular Function (MF), with the top 10 enriched terms in each category presented in Fig. 2G. KEGG pathway analysis (Fig. 2H) revealed the top 20 significantly enriched pathways. Genes associated with hyper-m7G lncRNAs were significantly showed strong enrichment related to cytoskeletal remodeling, cell adhesion, signal transduction, transmembrane transport, membrane localization, and metabolic regulation. These findings highlight their potential involvement in cellular migration, signal transduction, and metabolic alterations in tumors. Similarly, GO and KEGG pathway analyses of genes associated with hypo-m7G lncRNAs revealed significant enrichment in synaptic signaling, membrane transport, cytoskeletal structure, and calcium-related signal transduction pathways (**Supplementary Fig. 1A,B**).

As shown in Table 1, the top ten lncRNAs exhibiting the most significant changes in m7G methylation, both hypermethylated and hypomethylated, are listed.

3.3 Integrated m7G Methylation and Expression Profiling of lncRNAs Reveals Oncogenic Pathways in OSCC

Differential expression analysis of lncRNAs was conducted using HTSeq software, identifying 266 upregulated and 303 downregulated lncRNAs based on the thresholds of $p < 0.05$ and $|\log_2 \text{FC}| > 2$ (Fig. 3A,B). By intersecting the transcriptome and epitranscriptome datasets, we identified 80 lncRNAs that exhibited concurrent hyper-m7G modification and upregulation, while 103 lncRNAs were both hypomethylated and downregulated (Fig. 3C).

GO and KEGG pathway enrichment analyses were conducted for genes associated with dysregulated lncRNAs. The results showed that genes associated with upregulated lncRNAs were significantly enriched in diverse metabolic processes, pathways related to cell adhesion and migration, along with a variety of signaling pathways (Fig. 3D,E). Meanwhile, GO and KEGG analyses of genes associated with downregulated lncRNAs, showing significant enrichment in muscle system processes, cytoskeletal organization, and cardiomyopathy-related pathways (**Supplementary Fig. 2A,B**).

Furthermore, GO and KEGG enrichment analyses of genes associated with hyper-m7G-modified and upregulated lncRNAs revealed significant enrichment in various biological pathways, including retinoic acid metabolism, xenobiotic and drug metabolism, the proteasome pathway, and cell adhesion-related processes such as focal adhesion and adherens junction. These findings suggest that such lncRNAs may be involved in regulating cellular metabolic activity, protein degradation mechanisms, and tumor cell adhesion and migration, potentially contributing to OSCC progression (Fig. 3F,G). In parallel, functional annotation (GO and KEGG) of the target genes linked to the concurrent hypo-m7G and downregulated lncRNAs highlighted a prominent involvement in pathways related to neuronal development, intracellular signaling and transport, calcium signaling, and chromatin remodeling (**Supplementary Fig. 2C,D**).

Taken together, the data suggest that lncRNAs exhibiting both hypermethylation and upregulation are closely associated with oncogenic pathways, implicating them as potential contributors to OSCC progression.

3.4 DPY19L1P1 is Identified as a Hyper-m7G-Modified lncRNA and Candidate Biomarker in OSCC

Given the well-established association between m7G hypermethylation and OSCC progression, we further analyzed the set of 80 lncRNAs that exhibited both increased m7G methylation and upregulated expression in OSCC tissues. Among these lncRNAs, 20 showed a fold change in m7G methylation greater than 100 (Table 2). To ensure

Table 1. Top 10 lncRNAs with the most significant fold changes in either hyper- or hypo-m7G in between OSCC tissues and normal tissues.

Transcript id	Gene name	FC value	*p*-value	Coordinates	Regulation
ENST00000443767	*TATDN2P1*	1210.4	7.3528×10^{-9}	chrX:44143162-44145492+	Hyper-m7G
uc004bit.1	*AX746484*	1140.3	3.5411×10^{-9}	chr9:117112777-117115409-	Hyper-m7G
ENST00000452051	*TM4SF19-AS1*	1020.7	1.1286×10^{-9}	chr3:196045221-196052441+	Hyper-m7G
ENST00000435770	*RPL36AP6*	994.7	3.2269×10^{-9}	chr9:110596790-110597110-	Hyper-m7G
ENST00000519041	*RP11-386D6.1*	893.6	4.9882×10^{-9}	chr8:87719775-87777251+	Hyper-m7G
ENST00000609973	*GRM4*	860.4	3.5150×10^{-9}	chr6:34021956-34100798-	Hyper-m7G
NR_110306	*LOC101929657*	837.7	1.0048×10^{-8}	chr13:52703031-52706859+	Hyper-m7G
NR_026790	*HCG11*	829.0	3.2564×10^{-9}	chr6:26521934-26527612+	Hyper-m7G
NR_024433	*LINC00926*	819.2	3.2771×10^{-9}	chr15:57592563-57599967+	Hyper-m7G
ENST00000526935	*CTD-3064C13.1*	808.6	3.1712×10^{-9}	chr11:22282755-22283802-	Hyper-m7G
ENST00000433383	*NEK4P1*	1015.7	5.3712×10^{-9}	chr21:18582787-18583665-	Hypo-m7G
ENST00000509669	*CTD-3179P9.1*	885.7	3.7330×10^{-9}	chr5:117260703-117542666+	Hypo-m7G
NR_027498	*COL18A1-AS1*	809.1	4.1420×10^{-9}	chr21:46839631-46844985-	Hypo-m7G
ENST00000609206	*CTA-268H5.14*	774.0	3.7204×10^{-9}	chr22:45658166-45659466-	Hypo-m7G
ENST00000464333	*SFI1*	766.1	3.8445×10^{-9}	chr22:32010357-32014533+	Hypo-m7G
ENST00000445341	*MSANTD2P1*	732.7	4.0893×10^{-9}	chr21:24473545-24475396+	Hypo-m7G
ENST00000507903	*RP11-586E1.1*	723.9	5.5059×10^{-9}	chr5:62318746-62319316-	Hypo-m7G
ENST00000393388	*RP11-320N7.1*	710.4	4.5655×10^{-9}	chr12:4219194-4227298-	Hypo-m7G
NR_103535	*NEXN-AS1*	708.3	6.9869×10^{-9}	chr1:78347033-78355224-	Hypo-m7G
ENST00000480002	*CACNG2*	665.3	4.0822×10^{-9}	chr22:36980536-36981501-	Hypo-m7G

lncRNAs, long non-coding RNAs; m7G, N7-methylguanosine; OSCC, oral squamous cell carcinoma.

the specificity of non-coding RNA candidates, we examined all transcripts generated by each gene and retained only eight lncRNAs whose transcripts were classified as non-coding, whereas the remaining genes contained one or more protein-coding transcripts.

These eight lncRNAs were further analyzed using multiple public databases, including GEPIA3 (https://gepia3.bioinfoliu.com/) [33], ENCORI (https://rnasysu.com/encori/panCancer.php) [34], cProSite (https://cprosite.ccr.cancer.gov) [35], TIMER3 (https://compbio.cn/timer3/) [36], to evaluate their expression patterns in HNSCC. The results revealed that *DPY19L1P1*, *BLACAT1*, *ANKRD36BP2*, and *MIR17HG* were highly expressed in the TCGA-HNSC cohort (Fig. 4A–D; **Supplementary Fig. 3A,B**). To further explore regulatory mechanisms, the correlation between these candidate lncRNAs and METTL1/WDR4 was assessed. Among them, *DPY19L1P1* and *MIR17HG* exhibited a significant positive correlation with *METTL1* expression (Fig. 4E; **Supplementary Fig. 3C**). Notably, *DPY19L1P1* showed the most prominent m7G hypermethylation and was thus prioritized as the top candidate for further investigation. In addition, analysis using the cProSite dataset revealed that *DPY19L1P1* expression was also positively correlated with both *METTL1* and *WDR4* (Fig. 4F,G), suggesting a potential regulatory relationship.

Expression data from the GDC portal (https://portal.gdc.cancer.gov) [37] and the UCSC Xena Browser (http://xena.ucsc.edu/) [38] further confirmed that *DPY19L1P1* is significantly upregulated in HNSCC tissues (Fig. 4H; **Supplementary Fig. 3D,E**). Moreover, receiver operating characteristic (ROC) curve analysis yielded an AUC of 0.7848, indicating that diagnostic potential of *DPY19L1P1* in HNSCC (Fig. 4I). Elevated *DPY19L1P1* expression correlated significantly with higher clinical stage (Stage IV) and poor tumor grade (Fig. 4J).

Collectively, these results suggest that *DPY19L1P1* is a hyper-m7G-modified lncRNA with potential clinical utility as a diagnostic and prognostic biomarker in HNSCC.

3.5 DPY19L1P1 Expression and m7G Modification are Post-Transcriptionally Regulated by METTL1/WDR4

The expression level of *DPY19L1P1* was evaluated across commonly used OSCC cell lines. The results showed that *DPY19L1P1* was markedly upregulated in OSCC cells, with CAL-27 and HN30 exhibiting the highest expression levels (Fig. 5A). Consequently, these two lines were adopted as model systems to elucidate how the m7G methyltransferases METTL1 and WDR4 influence both the expression and m7G modification of *DPY19L1P1*. In OSCC cell lines, knockdown or overexpression of METTL1 or WDR4 resulted in consistent changes in *DPY19L1P1* expression, indicating a regulatory relationship (Fig. 5B,C).

To further characterize the m7G methylation status of *DPY19L1P1*, m7G peaks within its transcripts were visualized in OSCC and normal tissues using Integrative Genomics Viewer (IGV) (Fig. 5D). On the basis of predictions from the m7G Hub V2.0 database combined with

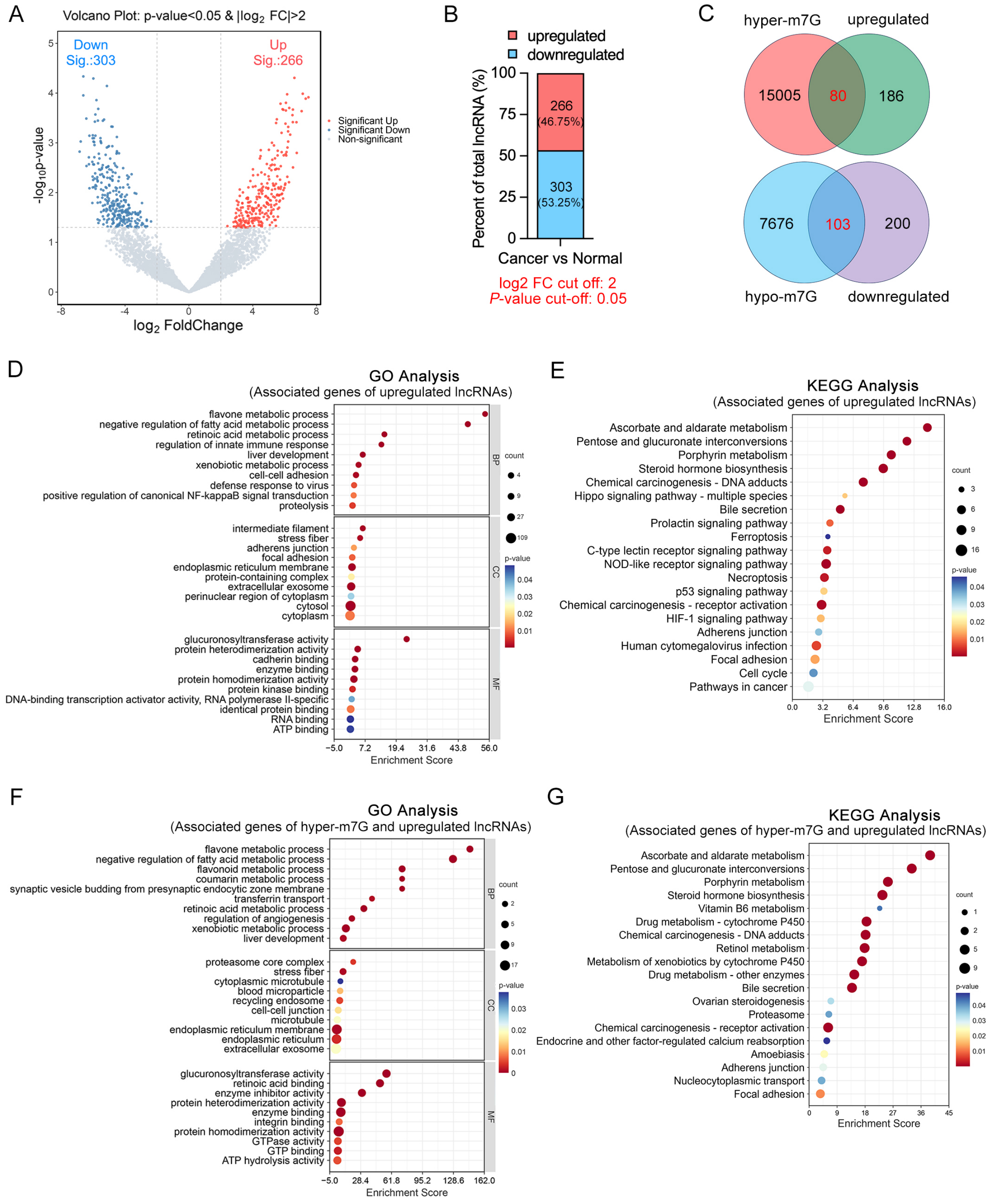

Fig. 3. Integrated analysis of differentially expressed and hyper-m7G-modified lncRNAs in OSCC. (A) Volcano plot displaying the differentially expressed lncRNAs in OSCC tissues compared to adjacent normal tissues. Red and blue dots represent significantly upregulated and downregulated lncRNAs, respectively ($|\log_2 \text{FC}| > 2, p < 0.05$). (B) Proportion of significantly upregulated (266; 46.75%) and downregulated (303; 53.25%) lncRNAs between tumor and normal tissues. (C) Venn diagrams illustrating the overlap between hyper-m7G-modified and upregulated lncRNAs (top), and between hypo-m7G-modified and downregulated lncRNAs (bottom), suggesting potential regulatory associations between m7G methylation and lncRNA expression. (D,E) GO and KEGG enrichment analyses of genes associated with significantly upregulated lncRNAs, indicating their involvement in metabolic processes, immune regulation, signaling pathways, and tumor-related pathways. (F,G) GO and KEGG enrichment analyses of genes associated with both hyper-m7G-modified and upregulated lncRNAs, highlighting enriched pathways related to metabolism, protein processing, stress response, and cancer-related signaling.

Table 2. Top 20 lncRNAs with the most significant fold change (FC >100) among hyper-m7G-modified and upregulated lncRNAs in OSCC tissues compared with normal tissues.

Transcript id	Gene name	FC value	*p*-value	Coordinates	Gene type[1]	Source
ENST00000467041	*SSR2*	347.9	5.2124×10^{-9}	chrX:44143162-44145492+	Mixed	gencode
ENST00000411812	*RNF216*	312.9	3.2279×10^{-9}	chr9:117112777-117115409-	Mixed	gencode
ENST00000526172	*C1orf106*	296.6	4.2345×10^{-9}	chr3:196045221-196052441+	Mixed	gencode
uc031qjh.1	*JX088243*	272.3	3.8232×10^{-9}	chr9:110596790-110597110-	Non-coding	UCSC
ENST00000481194	*CCM2*	250.8	3.1880×10^{-9}	chr8:87719775-87777251+	Mixed	gencode
uc002snv.4	*BC024248*	240.1	3.5411×10^{-9}	chr6:34021956-34100798-	Non-coding	UCSC
NR_036680	*DPY19L1P1*	234.8	3.5779×10^{-9}	chr13:52703031-52706859+	pseudogene	RefSeq
NR_103783	*BLACAT1*	229.1	7.0597×10^{-10}	chr6:26521934-26527612+	LncRNA	RefSeq
ENST00000592582	*SEH1L*	183.2	1.9911×10^{-9}	chr15:57592563-57599967+	Mixed	gencode
ENST00000551334	*CTD-2314B22.3*	177.7	3.6684×10^{-9}	chr11:22282755-22283802-	LncRNA	gencode
ENST00000525379	*KDM2A*	177.6	1.1450×10^{-9}	chr21:18582787-18583665-	Mixed	gencode
ENST00000421951	*ANKRD36BP2*	164.4	9.2036×10^{-10}	chr5:117260703-117542666+	pseudogene	gencode
ENST00000541795	*RAB6A*	163.4	3.5101×10^{-9}	chr21:46839631-46844985-	Mixed	gencode
ENST00000435097	*FAM83H-AS1*	157.1	3.2174×10^{-9}	chr22:45658166-45659466-	Mixed	gencode
ENST00000493456	*NUP50*	133.1	2.9514×10^{-9}	chr22:32010357-32014533+	Mixed	gencode
uc003skl.1	*AK127339*	126.5	3.9081×10^{-9}	chr21:24473545-24475396+	Non-coding	UCSC
ENST00000483509	*KIAA1841*	121.9	4.1191×10^{-9}	chr5:62318746-62319316-	Mixed	gencode
NR_027350	*MIR17HG*	110.7	6.8074×10^{-10}	chr12:4219194-4227298-	ncRNA	RefSeq
ENST00000486208	*GGNBP2*	109.4	9.2636×10^{-9}	chr1:78347033-78355224-	Mixed	gencode
ENST00000473949	*ARF1*	103.0	2.1545×10^{-8}	chr22:36980536-36981501-	Mixed	gencode

[1] Mixed indicates that the gene locus contains both protein-coding and noncoding transcript isoforms.

MeRIP-seq data, exon 14 of *DPY19L1P1* was identified as the major m7G-modified region of *DPY19L1P1*, spanning 126 base pairs (Fig. 5E). Primers targeting the peak region were designed accordingly (**Supplementary Table 1**), and MeRIP-qPCR analysis confirmed that *DPY19L1P1* is hyper-m7G-modified in OSCC cells (Fig. 5F). Importantly, m7G enrichment on *DPY19L1P1* decreased significantly following METTL1 or WDR4 knockdown, whereas overexpression of either enzyme enhanced m7G methylation (Fig. 5G,H). Together, these findings indicate that the METTL1/WDR4 methyltransferase complex modulates both the expression and m7G methylation level of *DPY19L1P1* in OSCC.

To further investigate the regulatory mechanism by which METTL1/WDR4 modulates *DPY19L1P1* expression, we examined the levels of precursor and mature transcripts. Knockdown of METTL1 or WDR4 significantly increased the expression of *DPY19L1P1* precursor RNA (Fig. 5I), while markedly reducing the levels of mature RNA (Fig. 5J), resulting in a notable elevation of the precursor-to-mature RNA ratio, indicative of impaired splicing efficiency (Fig. 5K). These findings suggest that METTL1/WDR4 regulates *DPY19L1P1* at the post-transcriptional level by modulating its splicing efficiency.

3.6 DPY19L1P1 Promotes OSCC Progression and Mediates METTL1/WDR4-Driven Oncogenic Effects

Nuclear/cytoplasmic fractionation analysis in CAL-27 cells revealed that *DPY19L1P1* was predominantly localized in the nucleus, with a nuclear/cytoplasmic distribution ratio of 75.06 ± 2.52% (nuclear) versus 24.94 ± 2.52% (cytoplasmic) (Fig. 6A). Consistently, FISH analysis further confirmed the nuclear enrichment of *DPY19L1P1* in HN30 cells (Fig. 6B). To elucidate the functional role of *DPY19L1P1* in OSCC, we performed both loss- and gain-of-function assays. Transfection with SS-DPY19L1P1 effectively silenced *DPY19L1P1* expression in CAL-27 cells (**Supplementary Fig. 4A**), whereas transfection with an overexpression plasmid significantly increased its expression in HN30 cells (**Supplementary Fig. 4B**). CCK-8 assay revealed that knockdown of *DPY19L1P1* inhibited CAL-27 cell proliferation (Fig. 6C), whereas its overexpression enhanced proliferation in HN30 cells (Fig. 6D). Similarly, Transwell migration assay revealed that *DPY19L1P1* silencing significantly inhibited migration of CAL-27 cells (Fig. 6E), while its overexpression promoted migration in HN30 cells (Fig. 6F). Moreover, among the three ASOs included in the Smart Silencer, ASO-DPY19L1P1-1 was identified as having the most potent knockdown efficiency (**Supplementary Fig. 4C**). This ASO (hereafter referred to as ASO-DPY19L1P1) was selected for intratumoral injection in an *in vivo* xenograft model. The results demonstrated that silencing *DPY19L1P1 in vivo* significantly suppressed tumor growth (Fig. 6G,H), further supporting its oncogenic role in OSCC.

It has been well documented that METTL1/WDR4 functions as a key driver in facilitating the growth and motility of OSCC cells [7]. To determine whether

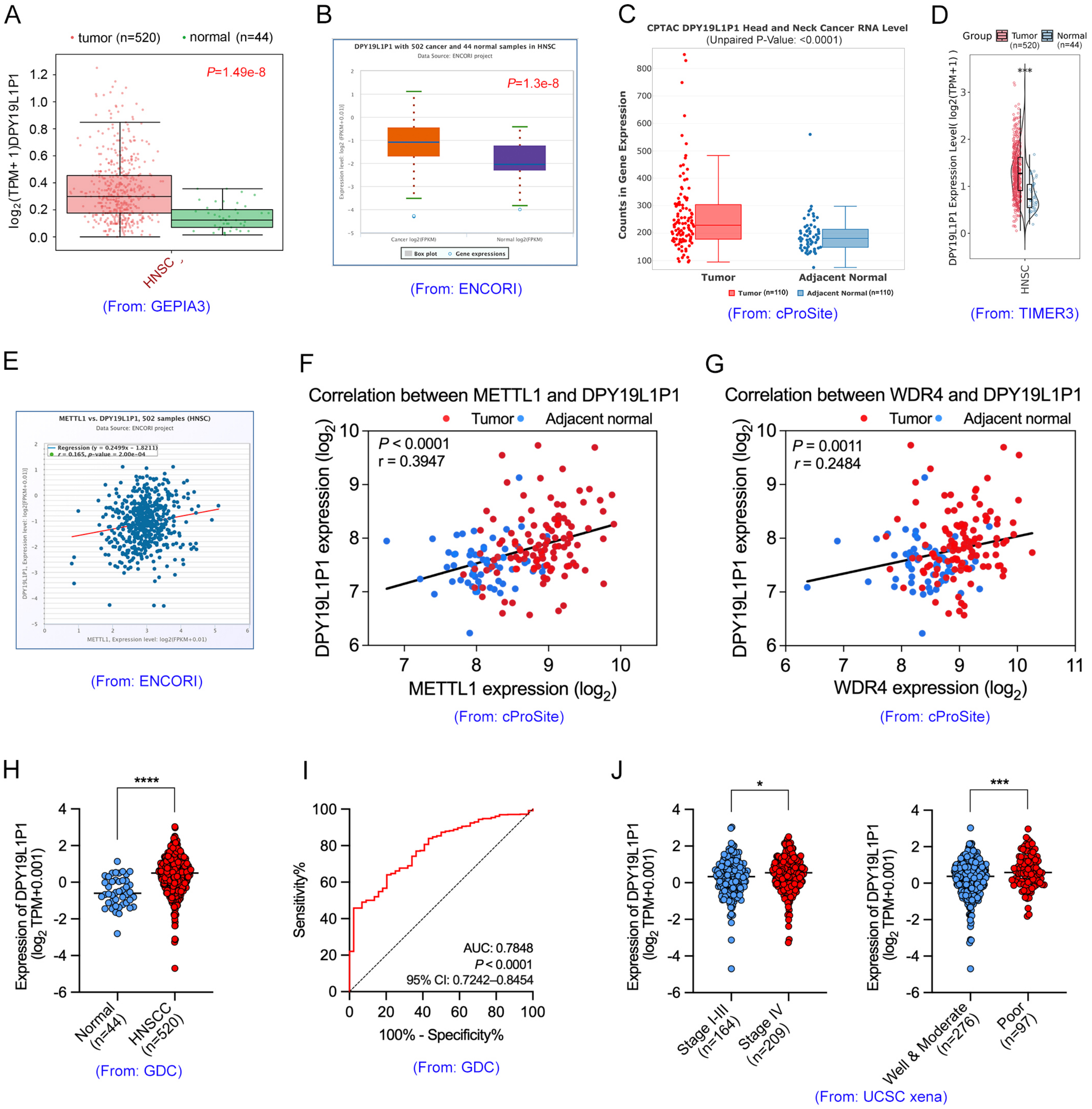

Fig. 4. Clinical characterization and expression patterns of *DPY19L1P1* in OSCC. (A–D) *DPY19L1P1* expression was significantly upregulated in head and neck squamous cell carcinoma (HNSCC) tissues compared to normal tissues, as shown by GEPIA3 (A), ENCORI (B), cProSite (C), and TIMER3 (D) databases. (E) Pearson correlation analysis based on the ENCORI database revealed a strong positive association between METTL1 and *DPY19L1P1* expression levels in HNSCC samples. (F,G) Correlation analysis using cProSite showed a positive relationship between *DPY19L1P1* expression and METTL1 (F) or WDR4 (G) expression in tumor tissues. (H) Analysis of the GDC (TCGA) database further confirmed the elevated expression of *DPY19L1P1* in HNSCC tissues (n = 520) versus normal controls (n = 44). (I) Receiver operating characteristic (ROC) curve analysis revealed that *DPY19L1P1* has good diagnostic performance for HNSCC, with an AUC of 0.7848 (95% CI: 0.7242–0.8454, $p < 0.0001$). (J) *DPY19L1P1* expression was significantly higher in stage IV tumors compared to stage I–III tumors and in poorly differentiated tumors compared to well- and moderately differentiated tumors, based on UCSC Xena data. AUC, area under the ROC curve. *$p < 0.05$, ***$p < 0.001$, ****$p < 0.0001$.

DPY19L1P1 functions downstream of METTL1/WDR4, we conducted rescue experiments. Overexpression of *DPY19L1P1* partially reversed the reduced proliferative (Fig. 6I,J) and migratory (Fig. 6K,L) abilities caused by

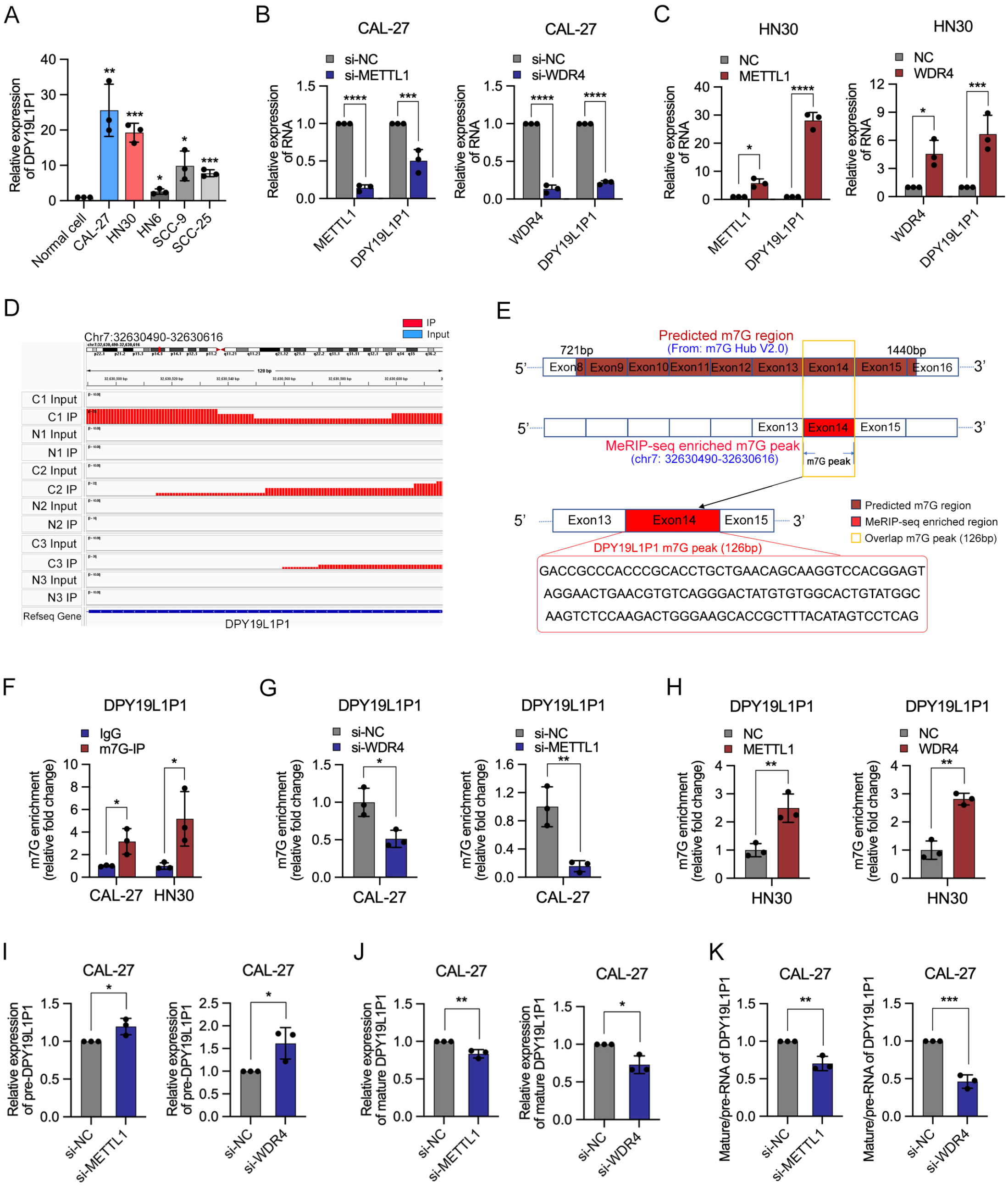

Fig. 5. METTL1/WDR4 regulates the expression and m7G modification of *DPY19L1P1* in OSCC. (A) qPCR analysis of *DPY19L1P1* expression in normal oral epithelial cells and OSCC cell lines (CAL-27, HN30, HN6, SCC9, and SCC25). (B) qPCR showing that knockdown of METTL1 or WDR4 significantly reduced *DPY19L1P1* expression in CAL-27 cells. (C) qPCR showing that overexpression of METTL1 or WDR4 significantly increased *DPY19L1P1* expression in HN30 cells. (D) Integrative Genomics Viewer (IGV) visualization of MeRIP-seq reads mapping to the *DPY19L1P1* locus in OSCC tissues (C1–C3) and normal tissues (N1–N3), revealing enriched m7G peaks specifically in OSCC samples. (E) Schematic illustration of the predicted m7G modification sites in the *DPY19L1P1* transcript based on m7G Hub data and MeRIP-seq peaks, highlighting the overlapping region and its sequence. (F) MeRIP-qPCR showing significant enrichment of m7G-modified *DPY19L1P1* relative to IgG in CAL-27 and HN30 cells. (G) MeRIP-qPCR showing reduced m7G enrichment of *DPY19L1P1* following METTL1 or WDR4 knockdown in CAL-27 cells. (H) MeRIP-qPCR showing increased m7G enrichment of *DPY19L1P1* following METTL1 or WDR4 overexpression in HN30 cells. (I) qPCR analysis of precursor *DPY19L1P1* transcript level after METTL1 or WDR4 knockdown in CAL-27 cells. (J) qPCR analysis of mature *DPY19L1P1* transcript levels following METTL1 or WDR4 knockdown. (K) Splicing efficiency represented by the ratio of mature *DPY19L1P1* to precursor *DPY19L1P1* transcripts. siRNA, small interfering RNA; NC, Negative Control; IP, immunoprecipitation; pre-*DPY19L1P1*, precursor *DPY19L1P1*. *$p < 0.05$, **$p < 0.01$, ***$p < 0.001$, ****$p < 0.0001$.

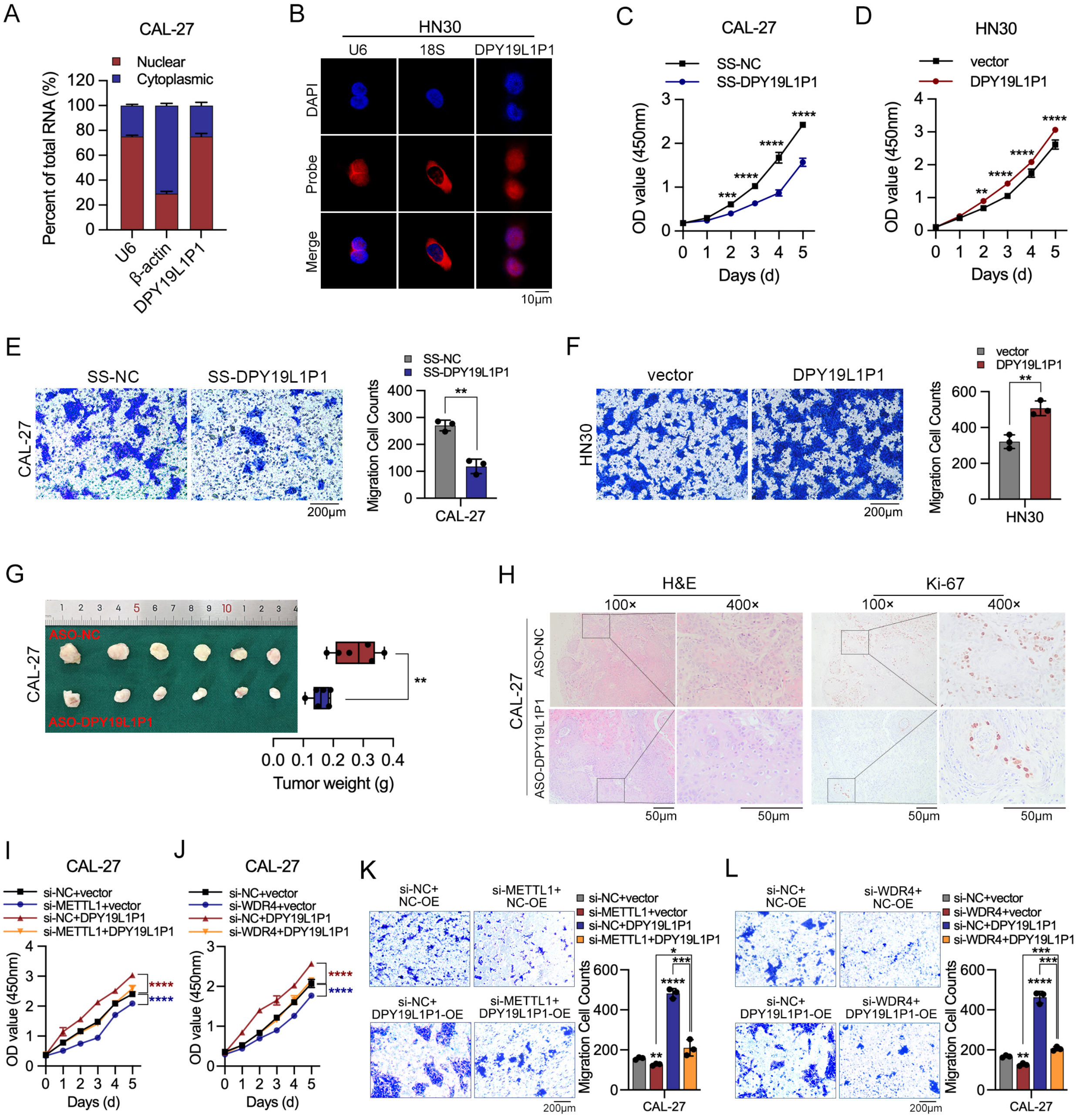

Fig. 6. *DPY19L1P1* enhances OSCC progression and functionally cooperates with METTL1/WDR4. (A) The subcellular localization of *DPY19L1P1* was determined by nuclear/cytoplasmic fractionation in CAL-27 cells. U6 and β-actin served as nuclear and cytoplasmic controls, respectively. (B) The subcellular localization of *DPY19L1P1* was determined by nuclear/cytoplasmic fractionation in fluorescence *in situ* hybridization (FISH) in HN30 cells. U6 and 18S rRNA served as nuclear and cytoplasmic controls, respectively. Scale bar: 10 µm. (C,D) The effect of *DPY19L1P1* on OSCC cell proliferation was determined via CCK-8 assays in *DPY19L1P1*-knockdown CAL-27 cells and *DPY19L1P1*-overexpressing HN30 cells. (E,F) The effect of *DPY19L1P1* on OSCC cell migration was assessed using Transwell assays in *DPY19L1P1*-knockdown CAL-27 cells and *DPY19L1P1*-overexpressing HN30 cells. Scale bar: 200 µm. (G) Subcutaneous xenograft model in BALB/c nude mice using CAL-27 cells transfected with ASO-NC or ASO-*DPY19L1P1*. Representative tumor images and tumor weights after 28 days are shown. (H) Histological analysis of xenograft tumors by HE and Ki-67 staining. Images were acquired at 100× and 400× magnification. Scale bar: 50 µm. (I,J) CCK-8 assays assessing the effect of *DPY19L1P1* overexpression on cell proliferation in CAL-27 cells with METTL1 (I) or WDR4 (J) knockdown. (K,L) Transwell migration assays evaluating the effect of *DPY19L1P1* overexpression on cell migration in CAL-27 cells with METTL1 (K) or WDR4 (L) knockdown. Scale bar = 200 µm. SS, Smart Silencer; ASO, antisense oligonucleotide; H&E, hematoxylin and eosin. *$p < 0.05$, **$p < 0.01$, ***$p < 0.001$, ****$p < 0.0001$.

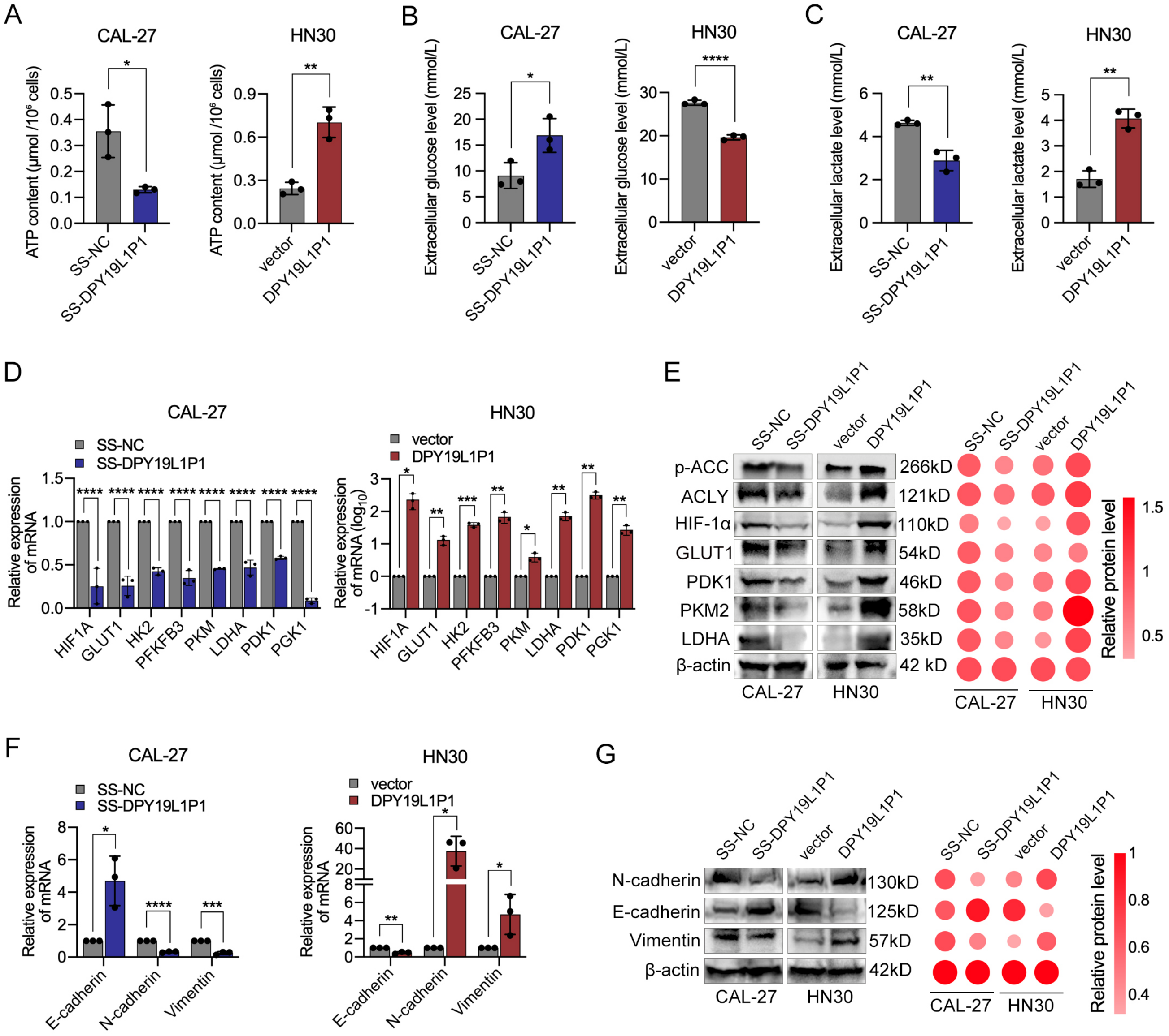

Fig. 7. *DPY19L1P1* promotes glycolytic metabolism and EMT in OSCC cells. (A) Intracellular ATP levels were measured in CAL-27 cells with *DPY19L1P1* knockdown and HN30 cells with *DPY19L1P1* overexpression. (B) Glucose uptake was assessed in CAL-27 cells with *DPY19L1P1* knockdown and HN30 cells with *DPY19L1P1* overexpression. (C) Lactate production was quantified in CAL-27 cells with *DPY19L1P1* knockdown and HN30 cells with *DPY19L1P1* overexpression. (D) qPCR analysis of key glycolytic pathway genes (*HIF1A*, *GLUT1*, *HK2*, *PKM*, *LDHA*, etc.) in CAL-27 cells with *DPY19L1P1* knockdown and HN30 cells with *DPY19L1P1* overexpression. (E) Western blot analysis of glycolysis- and lipid metabolism–related proteins (HIF-1α, GLUT1, PDK1, PKM2, LDHA, p-ACC, and ACLY) in CAL-27 cells with *DPY19L1P1* knockdown and HN30 cells with *DPY19L1P1* overexpression. (F) qPCR analysis of EMT marker genes (E-cadherin, N-cadherin, and vimentin) in CAL-27 cells with *DPY19L1P1* knockdown and HN30 cells with *DPY19L1P1* overexpression. (G) Western blot analysis of EMT-related proteins (E-cadherin, N-cadherin, and vimentin) in CAL-27 cells with *DPY19L1P1* knockdown and HN30 cells with *DPY19L1P1* overexpression. *$p < 0.05$, **$p < 0.01$, ***$p < 0.001$, ****$p < 0.0001$.

METTL1 or WDR4 knockdown. These results support the notion that *DPY19L1P1* acts as a downstream effector of the METTL1/WDR4 complex, mediating its oncogenic effects in OSCC progression.

3.7 DPY19L1P1 Promotes Glycolytic Metabolic Reprogramming and EMT in OSCC

Given that previous GO and KEGG analyses revealed enrichment of hyper-m7G-modified and upregulated genes in functions and pathways related to metabolism and cell adhesion, we further investigated whether *DPY19L1P1* is involved in metabolic processes and EMT.

We first assessed changes in intracellular ATP levels following *DPY19L1P1* knockdown or overexpression. ATP quantification assays showed that silencing *DPY19L1P1* significantly reduced ATP levels in CAL-27 cells, whereas its overexpression markedly increased ATP production in HN30 cells, indicating that *DPY19L1P1* is involved in cellular energy metabolism (Fig. 7A). Furthermore, glucose uptake and lactate production assays confirmed that *DPY19L1P1* knockdown decreased glucose consumption and lactate generation, while its overexpression enhanced both parameters (Fig. 7B,C). These results suggest that *DPY19L1P1* promotes a shift toward glycolytic metabolism. In line with this, qPCR analysis revealed that *DPY19L1P1* overexpression upregulated the mRNA level of key glycolytic genes, including *HIF1A*, *GLUT1*, *HK2*, *PFKFB3*, *PKM*, *LDHA*, *PDK1*, and *PGK1* (Fig. 7D), implying a role in promoting aerobic glycolysis (the Warburg effect) and metabolic reprogramming in OSCC cells.

Consistently, Western blot analysis confirmed that *DPY19L1P1* positively regulates glycolytic markers (HIF-1α, GLUT1, PDK1, PKM2, LDHA) and lipogenesis-related proteins (p-ACC, ACLY), further supporting its functional involvement in tumor metabolic reprogramming (Fig. 7E).

Additionally, we investigated the role of *DPY19L1P1* in EMT. qPCR and Western blot analysis revealed that *DPY19L1P1* knockdown caused increased E-cadherin and decreased N-cadherin and vimentin expression, while its overexpression produced the opposite effect (Fig. 7F,G). These findings indicate that *DPY19L1P1* facilitates EMT progression in OSCC cells, potentially contributing to enhanced migratory and invasive capabilities.

4. Discussion

m7G modification is among the most prevalent post-transcriptional RNA modifications and plays a pivotal role in promoting malignant tumor progression by modulating RNA metabolism and gene expression [7,39]. METTL1 and WDR4, the key methyltransferases responsible for internal m7G methylation of mRNAs and lncRNAs, have been shown to contribute significantly to cancer progression, including in OSCC, where their overexpression correlates with poor prognosis [7,13,40].

Emerging evidence underscores the regulatory importance of m7G-modified lncRNAs in diverse cancer types, where they influence critical biological processes such as metabolic reprogramming, proliferation, and metastasis [41]. In particular, m7G-related lncRNAs have recently emerged as potential biomarkers prognostic and prediction of immune response in several malignancies, including colorectal, endometrial, lung, liver, bladder, and pancreatic cancers [42–47]. Although bioinformatics analyses have suggested similar roles for m7G-related lncRNAs in OSCC [18], direct experimental validation remains lacking.

In this study, we performed a comprehensive analysis of m7G-modified lncRNAs based on m7G MeRIP-seq and RNA-seq in paired OSCC and adjacent normal tissues. We found that lncRNAs with high m7G modification level were significantly enriched in OSCC tissues. Notably, peak lengths of m7G-modified regions differed significantly between tumor and normal samples, and hyper-m7G was the dominant modification pattern. Genes associated with hyper-m7G and/or upregulated lncRNAs were shown enrichment in pathways related to metabolism and cell migration, suggesting that these lncRNAs may play oncogenic roles in OSCC. However, we acknowledge the limited sample size (n = 3 pairs), which may affect representativeness and biological variability. Future studies involving larger clinical cohorts are needed to validate these findings.

Among the hyper-m7G-modified and upregulated lncRNAs, we focused on *DPY19L1P1*, which was clearly annotated as non-coding and exhibited the most prominent m7G peak signal in OSCC. *DPY19L1P1* is classified as an unprocessed pseudogene of *DPY19L1*, a gene encoding a C-mannosyltransferase that catalyzes the C-mannosylation of tryptophan residues in proteins and may influence cancer cell behavior by modifying receptor tyrosine kinases [48]. Despite the shared nomenclature, there is no evidence indicating any regulatory or functional interaction between *DPY19L1P1* and *DPY19L1*. Functionally, *DPY19L1P1* acts as a regulatory lncRNA and has been implicated in various disease contexts, including cryptococcal meningitis [49], acute myeloid leukemia [50], and epicardial fat tissue inflammation associated with atrial fibrillation [51]. However, to date, no studies have explored the functional role of DPY19L1P1 in OSCC or other solid tumors.

Our data demonstrate that *DPY19L1P1* is significantly upregulated in OSCC and correlates with advanced tumor stage and poor differentiation, suggesting clinical significance and diagnostic value. Mechanistically, METTL1 and WDR4 cooperatively regulate both the expression and m7G methylation level of *DPY19L1P1*, likely by enhancing its splicing efficiency. This aligns with known post-transcriptional effects of m7G modification and provides a plausible explanation for *DPY19L1P1* overexpression in OSCC. Functional assays confirmed that *DPY19L1P1* promotes OSCC cell proliferation, migration, and metabolic reprogramming, consistent with the known oncogenic roles of METTL1/WDR4 [7,14]. Notably, *DPY19L1P1* was predominantly localized in the nucleus, where it transcriptionally modulated EMT and metabolic genes. This suggests a mechanism involving nuclear lncRNA-mediated recruitment of transcription factors or RNA-binding proteins to specific promoters [52]. However, this hypothesis warrants further investigation.

Although our findings indicate that *DPY19L1P1* functions downstream of METTL1/WDR4 in OSCC, whether its oncogenic role is directly dependent on m7G modification remains to be fully determined. In future studies, we aim to map the precise m7G modification sites on *DPY19L1P1* and determine whether the oncogenic activity of *DPY19L1P1* is dependent on METTL1/WDR4-mediated m7G methylation.

Importantly, we recognize that m7G is not the only modification potentially regulating *DPY19L1P1*. Systematic profiling of its full epitranscriptomic landscape will be crucial to explore potential crosstalk among different RNA modifications. Such research will deepen our understanding of lncRNA-mediated oncogenesis and may uncover new therapeutic strategies targeting RNA modifications.

5. Conclusion

This study systematically characterized the m7G methylation landscape of lncRNAs in OSCC and identified a subset of lncRNAs that were both highly expressed and hyper-m7G-modified in tumor tissues. These lncRNAs were closely associated with OSCC progression, particularly through pathways involving metabolic reprogramming and EMT. Among them, *DPY19L1P1* was identified as a representative hyper-m7G-modified oncogenic lncRNA, regulated by the METTL1/WDR4 complex, and shown to promote OSCC cell proliferation, migration, and glycolysis. These findings suggest that m7G-modified lncRNAs—particularly *DPY19L1P1*—may serve as potential biomarkers and treatment targets in OSCC.

Abbreviations

m7G, N7-methylguanosine; OSCC, oral squamous cell carcinoma; lncRNA, long non-coding RNA; METTL1, methyltransferase-like 1; WDR4, WD repeat domain 4; MeRIP-seq, methylated RNA immunoprecipitation sequencing; ECL, enhanced chemiluminescence; GO, Gene Ontology; BP, biological process; CC, cellular component; MF, molecular function; KEGG, Kyoto Encyclopedia of Genes and Genomes; FC, fold change; qPCR, quantitative real-time PCR; FISH, Fluorescence *In Situ* Hybridization; CCK-8, Cell Counting Kit-8; m6A, N6-methyladenosine; m1A, N1-methyladenosine; m5C, 5-methylcytosine; SS, Smart Silencer; HNSCC, head and neck squamous cell carcinoma; tRNA, transfer RNA; EMT, epithelial–mesenchymal transition; HE, Hematoxylin and Eosin; ASO, antisense oligonucleotide; siRNA, small interfering RNA; AUC, area under the ROC curve; ROC, receiver operating characteristic; IGV, Integrative Genomics Viewer.

Availability of Data and Materials

The datasets used and analyzed during the current study are available from the corresponding author on reasonable request.

Author Contributions

YJ conceived the project, designed the research and contributed to the manuscript preparation. KL and HG performed the research. SB, HX and RZ performed the data analysis. JH, YW and YZ contributed to data acquisition and manuscript revision. All authors contributed to editorial changes in the manuscript. All authors read and approved the final manuscript. All authors have participated sufficiently in the work and agreed to be accountable for all aspects of the work.

Ethics Approval and Consent to Participate

Tissue samples for research were collected in accordance with the Declaration of Helsinki and were approved by the Medical Ethics Committee of Weifang Medical University (Ethics No. 2022YX007). Informed consent was obtained from all patients. All animal studies were approved by the Animal Care and Use Committee of Weifang Medical University (Approval No. 2023SDL332). All animal experiments were conducted in accordance with the ARRIVE guidelines and the principles of the 3Rs (Replacement, Reduction, and Refinement). Weifang Medical University has since been renamed Shandong Second Medical University, and the corresponding ethics committees have been institutionally renamed accordingly. All approvals remain fully valid under the original protocols.

Acknowledgment

The authors wish to thank Ning Song and Minmin Li for their assistance in image organization.

Funding

This study was supported by grants from Shandong Provincial Natural Science Foundation (ZR2023LSW019), the Graduate Student Research Grant from Shandong Second Medical University (2024YJSCX004, 2023YJSCX005), and College students Innovation and Entrepreneurship Training Program of Shandong Second Medical University (X2025205, X2025206, X2025208).

Conflict of Interest

The authors declare no conflict of interest.

Supplementary Material

Supplementary material associated with this article can be found, in the online version, at https://doi.org/10.31083/FBL48929.

References

[1] Johnson DE, Burtness B, Leemans CR, Lui VWY, Bauman JE, Grandis JR. Head and neck squamous cell carcinoma. Nature Reviews. Disease Primers. 2020; 6: 92. https://doi.org/10.1038/s41572-020-00224-3.

[2] Mohamad I, Glaun MDE, Prabhash K, Busheri A, Lai SY,

Noronha V, *et al*. Current Treatment Strategies and Risk Stratification for Oral Carcinoma. American Society of Clinical Oncology Educational Book. American Society of Clinical Oncology. Annual Meeting. 2023; 43: e389810. https://doi.org/10.1200/EDBK_389810.

[3] Li H, Zhang Y, Xu M, Yang D. Current trends of targeted therapy for oral squamous cell carcinoma. Journal of Cancer Research and Clinical Oncology. 2022; 148: 2169–2186. https://doi.org/10.1007/s00432-022-04028-8.

[4] Roundtree IA, Evans ME, Pan T, He C. Dynamic RNA Modifications in Gene Expression Regulation. Cell. 2017; 169: 1187–1200. https://doi.org/10.1016/j.cell.2017.05.045.

[5] Tang Q, Li L, Wang Y, Wu P, Hou X, Ouyang J, *et al*. RNA modifications in cancer. British Journal of Cancer. 2023; 129: 204–221. https://doi.org/10.1038/s41416-023-02275-1.

[6] Cruz A, Joseph S. Interaction of the Influenza A Virus NS1 Protein with the 5′-m7G-mRNA·eIF4E·eIF4G1 Complex. Biochemistry. 2022; 61: 1485–1494. https://doi.org/10.1021/acs.biochem.2c00019.

[7] Chen J, Li K, Chen J, Wang X, Ling R, Cheng M, *et al*. Aberrant translation regulated by METTL1/WDR4-mediated tRNA N7-methylguanosine modification drives head and neck squamous cell carcinoma progression. Cancer Communications (London, England). 2022; 42: 223–244. https://doi.org/10.1002/cac2.12273.

[8] Zhang LS, Liu C, Ma H, Dai Q, Sun HL, Luo G, *et al*. Transcriptome-wide Mapping of Internal N^7-Methylguanosine Methylome in Mammalian mRNA. Molecular Cell. 2019; 74: 1304–1316.e8. https://doi.org/10.1016/j.molcel.2019.03.036.

[9] Zhao Z, Qing Y, Dong L, Han L, Wu D, Li Y, *et al*. QKI shuttles internal m^{7}G-modified transcripts into stress granules and modulates mRNA metabolism. Cell. 2023; 186: 3208–3226.e27. https://doi.org/10.1016/j.cell.2023.05.047.

[10] Sloan KE, Warda AS, Sharma S, Entian KD, Lafontaine DLJ, Bohnsack MT. Tuning the ribosome: The influence of rRNA modification on eukaryotic ribosome biogenesis and function. RNA Biology. 2017; 14: 1138–1152. https://doi.org/10.1080/15476286.2016.1259781.

[11] Li J, Li C, Li X, Chen Y, Li Z, Lin Y, *et al*. Establishment and assessment of an oral squamous cell carcinoma N7-methylguanosine methyltransferase associated microRNA prognostic model. Journal of Cancer. 2024; 15: 6022–6037. https://doi.org/10.7150/jca.98350.

[12] Fang H, He J, Du D, Wang X, Xu X, Lu L, *et al*. Deciphering the secret codes in N^7-methylguanosine modification: Context-dependent function of methyltransferase-like 1 in human diseases. Clinical and Translational Medicine. 2025; 15: e70240. https://doi.org/10.1002/ctm2.70240.

[13] Cheng W, Gao A, Lin H, Zhang W. Novel roles of METTL1/WDR4 in tumor via m^{7}G methylation. Molecular Therapy Oncolytics. 2022; 26: 27–34. https://doi.org/10.1016/j.omto.2022.05.009.

[14] Lu B, Li X, Miao W, Liu Q, Li R, Cui C, *et al*. Upregulation of WDR4 mediated by RBFOX2 promotes laryngeal cancer progression through the WDR4/m7G/lncRNA ZFAS1/RBFOX2 axis. Naunyn-Schmiedeberg's Archives of Pharmacology. 2025; 398: 7529–7543. https://doi.org/10.1007/s00210-024-03779-0.

[15] Bridges MC, Daulagala AC, Kourtidis A. LNCcation: lncRNA localization and function. The Journal of Cell Biology. 2021; 220: e202009045. https://doi.org/10.1083/jcb.202009045.

[16] Peng WX, Koirala P, Mo YY. LncRNA-mediated regulation of cell signaling in cancer. Oncogene. 2017; 36: 5661–5667. https://doi.org/10.1038/onc.2017.184.

[17] Niinuma T, Kitajima H, Sato T, Ogawa T, Ishiguro K, Kai M, *et al*. LINC02154 promotes cell cycle and mitochondrial function in oral squamous cell carcinoma. Cancer Science. 2025; 116: 393–405. https://doi.org/10.1111/cas.16379.

[18] Wang X, Dong W, Zhang Y, Huo F. m7G-related lncRNAs are potential biomarkers for predicting prognosis and immune responses in patients with oral squamous cell carcinoma. Frontiers in Genetics. 2022; 13: 1013312. https://doi.org/10.3389/fgene.2022.1013312.

[19] Sun D, Song N, Li M, Chen X, Zhang X, Yu Y, *et al*. Comprehensive analysis of circRNAs for N7-methylguanosine methylation modification in human oral squamous cell carcinoma. FASEB BioAdvances. 2023; 5: 305–320. https://doi.org/10.1096/fba.2023-00036.

[20] Li M, Song N, Sun D, Yu Y, Zheng W, Zhang X, *et al*. Transcriptome Mapping of the Internal N7-Methylguanosine Methylome in Messenger RNAs in Human Oral Squamous Cell Carcinoma. Frontiers in Bioscience (Landmark Edition). 2023; 28: 330. https://doi.org/10.31083/j.fbl2812330.

[21] Jiang Y, Wu K, Cao W, Xu Q, Wang X, Qin X, *et al*. Long noncoding RNA *KTN1-AS1* promotes head and neck squamous cell carcinoma cell epithelial-mesenchymal transition by targeting *miR-153-3p*. Epigenomics. 2020; 12: 487–505. https://doi.org/10.2217/epi-2019-0173.

[22] Jiang Y, Cao W, Wu K, Qin X, Wang X, Li Y, *et al*. LncRNA LINC00460 promotes EMT in head and neck squamous cell carcinoma by facilitating peroxiredoxin-1 into the nucleus. Journal of Experimental & Clinical Cancer Research: CR. 2019; 38: 365. https://doi.org/10.1186/s13046-019-1364-z.

[23] Martin M. Cutadapt removes adapter sequences from high-throughput sequencing reads. EMBnet. journal. 2011; 17: 10–12. https://doi.org/10.14806/ej.17.1.200.

[24] Kim D, Langmead B, Salzberg SL. HISAT: a fast spliced aligner with low memory requirements. Nature Methods. 2015; 12: 357–360. https://doi.org/10.1038/nmeth.3317.

[25] Zhang Y, Liu T, Meyer CA, Eeckhoute J, Johnson DS, Bernstein BE, *et al*. Model-based analysis of ChIP-Seq (MACS). Genome Biology. 2008; 9: R137. https://doi.org/10.1186/gb-2008-9-9-r137.

[26] Shen L, Shao NY, Liu X, Maze I, Feng J, Nestler EJ. diffReps: detecting differential chromatin modification sites from ChIP-seq data with biological replicates. PloS One. 2013; 8: e65598. https://doi.org/10.1371/journal.pone.0065598.

[27] Anders S, Pyl PT, Huber W. HTSeq–a Python framework to work with high-throughput sequencing data. Bioinformatics (Oxford, England). 2015; 31: 166–169. https://doi.org/10.1093/bioinformatics/btu638.

[28] Robinson MD, McCarthy DJ, Smyth GK. edgeR: a Bioconductor package for differential expression analysis of digital gene expression data. Bioinformatics (Oxford, England). 2010; 26: 139–140. https://doi.org/10.1093/bioinformatics/btp616.

[29] Dennis G, Jr, Sherman BT, Hosack DA, Yang J, Gao W, Lane HC, *et al*. DAVID: Database for Annotation, Visualization, and Integrated Discovery. Genome Biology. 2003; 4: P3. https://doi.org/10.1186/gb-2003-4-5-p3.

[30] Zhang H, Meltzer P, Davis S. RCircos: an R package for Circos 2D track plots. BMC Bioinformatics. 2013; 14: 244. https://doi.org/10.1186/1471-2105-14-244.

[31] Bailey TL. STREME: accurate and versatile sequence motif discovery. Bioinformatics (Oxford, England). 2021; 37: 2834–2840. https://doi.org/10.1093/bioinformatics/btab203.

[32] Pang B, Wu N, Guan R, Pang L, Li X, Li S, *et al*. Overexpression of RCC2 Enhances Cell Motility and Promotes Tumor Metastasis in Lung Adenocarcinoma by Inducing Epithelial-Mesenchymal Transition. Clinical Cancer Research: an Official Journal of the American Association for Cancer Research. 2017; 23: 5598–5610. https://doi.org/10.1158/1078-0432.CCR-16-2909.

[33] Tang Z, Li C, Kang B, Gao G, Li C, Zhang Z. GEPIA: a web

server for cancer and normal gene expression profiling and interactive analyses. Nucleic Acids Research. 2017; 45: W98–W102. https://doi.org/10.1093/nar/gkx247.

[34] Li JH, Liu S, Zhou H, Qu LH, Yang JH. starBase v2.0: decoding miRNA-ceRNA, miRNA-ncRNA and protein-RNA interaction networks from large-scale CLIP-Seq data. Nucleic Acids Research. 2014; 42: D92–D97. https://doi.org/10.1093/nar/gkt1248.

[35] Wang D, Qian X, Du YCN, Sanchez-Solana B, Chen K, Kanigicherla M, *et al*. cProSite: A web based interactive platform for online proteomics, phosphoproteomics, and genomics data analysis. Journal of Biotechnology and Biomedicine. 2023; 6: 573–578. https://doi.org/10.26502/jbb.2642-91280119.

[36] Cui H, Zhao G, Lu Y, Zuo S, Duan D, Luo X, *et al*. TIMER3: an enhanced resource for tumor immune analysis. Nucleic Acids Research. 2025; 53: W534–W541. https://doi.org/10.1093/nar/gkaf388.

[37] Grossman RL, Heath AP, Ferretti V, Varmus HE, Lowy DR, Kibbe WA, *et al*. Toward a Shared Vision for Cancer Genomic Data. The New England Journal of Medicine. 2016; 375: 1109–1112. https://doi.org/10.1056/NEJMp1607591.

[38] Goldman MJ, Craft B, Hastie M, Repečka K, McDade F, Kamath A, *et al*. Visualizing and interpreting cancer genomics data via the Xena platform. Nature Biotechnology. 2020; 38: 675–678. https://doi.org/10.1038/s41587-020-0546-8.

[39] Ma J, Han H, Huang Y, Yang C, Zheng S, Cai T, *et al*. METTL1/WDR4-mediated m^7G tRNA modifications and m^7G codon usage promote mRNA translation and lung cancer progression. Molecular Therapy: the Journal of the American Society of Gene Therapy. 2021; 29: 3422–3435. https://doi.org/10.1016/j.ymthe.2021.08.005.

[40] Zhang X, Chen Y, Li M, Zhou X, Song Q. METTL1 in human cancers: recognition of their functions, mechanisms and therapeutic value. Oncology Reviews. 2025; 19: 1637372. https://doi.org/10.3389/or.2025.1637372.

[41] Shi M, Zhu S, Sun L, Hu J, Li H, Dai W, *et al*. Transcriptome-Wide Dynamics of m7G-Related LncRNAs during the Progression from HBV Infection to Hepatocellular Carcinoma. Frontiers in Bioscience (Landmark Edition). 2023; 28: 339. https://doi.org/10.31083/j.fbl2812339.

[42] Liu L, Wu Y, Chen W, Li Y, Yu J, Zhang G, *et al*. The m7G-Related Long Noncoding RNA Signature Predicts Prognosis and Indicates Tumour Immune Infiltration in Colon Cancer. Frontiers in Genetics. 2022; 13: 892589. https://doi.org/10.3389/fgene.2022.892589.

[43] Sun J, Li L, Chen H, Gan L, Guo X, Sun J. Identification and Validation of an m7G-Related lncRNAs Signature for Prognostic Prediction and Immune Function Analysis in Endometrial Cancer. Genes. 2022; 13: 1301. https://doi.org/10.3390/genes13081301.

[44] Pan J, Huang Z, Lin H, Cheng W, Lai J, Li J. M7G-Related lncRNAs predict prognosis and regulate the immune microenvironment in lung squamous cell carcinoma. BMC Cancer. 2022; 22: 1132. https://doi.org/10.1186/s12885-022-10232-z.

[45] Yang L, Wang YR, Mou ZQ, Xiong PF, Deng K, Wen J, *et al*. A new prediction model of hepatocellular carcinoma based on N7-methylguanosine modification. BMC Gastroenterology. 2023; 23: 131. https://doi.org/10.1186/s12876-023-02757-9.

[46] Ren L, Yang X, Liu J, Wang W, Liu Z, Lin Q, *et al*. An innovative model based on N7-methylguanosine-related lncRNAs for forecasting prognosis and tumor immune landscape in bladder cancer. Cancer Cell International. 2023; 23: 85. https://doi.org/10.1186/s12935-023-02933-7.

[47] Lu J, Yang P, Yu L, Xie N, Wu Y, Li B. Identification of m7G-Related LncRNA Signature for Predicting Prognosis and Evaluating Tumor Immune Infiltration in Pancreatic Adenocarcinoma. Diagnostics (Basel, Switzerland). 2023; 13: 1697. https://doi.org/10.3390/diagnostics13101697.

[48] Mori K, Suzuki T, Waki U, Hayashi S, Kadono S, Kawahara R, *et al*. Identification of C-mannosylation in a receptor tyrosine kinase AXL. Glycobiology. 2024; 34: cwae096. https://doi.org/10.1093/glycob/cwae096.

[49] Zhang L, Fang WJ, Zhang KM, Jiang WW, Chen M, Liao WQ, *et al*. Long noncoding RNA expression profile from cryptococcal meningitis patients identifies DPY19L1p1 as a new disease marker. CNS Neuroscience & Therapeutics. 2019; 25: 772–782. https://doi.org/10.1111/cns.13109.

[50] Jian J, Wang X, Hao H, Ji C, Yuan C, Lu F. A Prognostic Model of Pseudogenes in Acute Myeloid Leukemia. Clinical Laboratory. 2023; 69: 938–947. https://doi.org/10.7754/Clin.Lab.2022.220825.

[51] Zheng H, Peng Y, Wang P, Su P, Zhao L. The integrative network of circRNA, miRNA and mRNA of epicardial adipose tissue in patients with atrial fibrillation. American Journal of Translational Research. 2022; 14: 6550–6562.

[52] Martianov I, Ramadass A, Serra Barros A, Chow N, Akoulitchev A. Repression of the human dihydrofolate reductase gene by a non-coding interfering transcript. Nature. 2007; 445: 666–670. https://doi.org/10.1038/nature05519.